

**Near infrared detection of decay
in post-mountain pine beetle lumber**
Rod Stirling
Mountain Pine Beetle working paper 2009-08

FPIInnovations – Forintek Division
2665 East Mall, Vancouver BC, V6T 1W5

Natural Resources Canada
Canadian Forest Service
Pacific Forestry Centre
506 West Burnside Road
Victoria, BC V8Z 1M5
Canada

MPBP Project #: 7.14

© Her Majesty the Queen in right of Canada 2009

Printed in Canada
2009

Library and Archives Canada Cataloguing in Publication

Stirling, Rod, 1977-

Near infrared detection of decay in post-mountain pine beetle lumber / Rod Stirling.

(Mountain pine beetle working paper ; 2009-08)

"MPBP Project # 7.14".

Includes bibliographical references.

Available also on the Internet.

Includes abstract in French.

ISBN 978-1-100-13140-5

Cat. no.: Fo143-3/2009-8E

1. Lumber--Testing. 2. Wood--Deterioration--Measurement. 3. Near infrared spectroscopy. 4. Lumber--Grading.
5. Mountain pine beetle--Economic aspects. I. Pacific Forestry Centre II. Title. III. Series: Mountain Pine Beetle
Initiative working paper 2009-08

SB945 M78 S74 2009

674.028'7

C2009-980168-X

Abstract

As mountain pine beetle-affected trees age in the forest, the incidence of decay increases and the type of decay is likely to change from limited amounts of heart-rot to increasing amounts of sap-rot. Given the scale of the current beetle epidemic in British Columbia, sawmills can expect to process increasing amounts of sap-rot in post-mountain pine beetle wood. In the normal process of grading lumber, a grader visually inspects the lumber, and places the small amounts of visibly decayed lumber into lower grades. However, increasing amounts of decay, the speed at which lumber is produced from a modern planer mill, and the presence of blue stain will make it more difficult for graders to visibly detect decay, other than advanced pocket rot or similar defects.

Automated grading systems that use colour cameras are able to do a reasonable job of detecting decay. This project investigated whether the use of visible/near infrared spectroscopy to identify decay in beetle-affected lumber could improve decay detection. Visible/near infrared spectroscopy was able to differentiate sound and decayed wood using a small beam centred on well-defined sound and decayed areas. However, when a larger beam was used, spectra often contained information from adjacent sound and decayed regions. This resulted in poorer classification. In all models the visible region had a greater influence than the near infrared region. In fact, models developed on colourimetric data alone ($L^*a^*b^*$) performed similarly to those developed over the entire visible/near infrared range. None of the developed models were able to detect decay more accurately than existing automated grading systems.

Keywords: mountain pine beetle, lumber grading, sap-rot, decay, visible/near infrared (NIR) spectroscopy

Résumé

À mesure que les arbres infestés par le dendroctone du pin ponderosa (DPP) vieillissent en forêt, le nombre de cas de pourriture augmente et il faut s'attendre à ce que la nature même de la pourriture évolue, d'une pourriture limitée au bois de cœur à une pourriture plus étendue de l'aubier. Vu l'étendue de l'infestation actuelle en Colombie-Britannique, les scieries peuvent s'attendre à une quantité croissante de pourriture de l'aubier dans le bois touché par le DPP. Dans le processus normal de classification du bois d'œuvre, un classeur inspecte visuellement le bois d'œuvre et classe la petite quantité de bois visiblement pourri dans les catégories inférieures. Cependant, en raison de l'augmentation du nombre de cas de pourriture, la vitesse à laquelle se fait le traitement du bois d'œuvre avec les raboteuses modernes et la présence de taches bleues, les classeurs auront plus de difficulté à détecter visuellement la pourriture, sauf en présence de pourriture alvéolaire avancée ou autres défauts similaires.

Les systèmes automatisés de classification de bois d'œuvre dotés de caméras couleur sont capables de faire un travail acceptable de détection de la pourriture. Le présent projet cherche à déterminer si l'utilisation de la spectroscopie visible ou proche infrarouge (NIR) pour détecter la pourriture dans le bois d'œuvre endommagé par le dendroctone du pin pourrait améliorer la détection de la pourriture. La spectroscopie visible/NIR était capable de différencier le bois sain du bois pourri en utilisant un petit faisceau centré sur des zones saines et pourries bien déterminées. Toutefois, lorsqu'on utilisait un faisceau plus grand, les spectres contenaient souvent des renseignements correspondant aux zones saines et pourries adjacentes. Par conséquent, la classification était moins bonne. Dans tous les modèles, la zone visible avait une influence plus grande que la zone NIR. En réalité, les modèles élaborés uniquement à partir de données chromatiques ($L^*a^*b^*$) ont donné les mêmes résultats que ceux élaborés sur la gamme visible/NIR complète. Aucun des modèles élaborés n'a été capable de détecter la pourriture plus précisément que les systèmes automatisés de classification actuels.

Mots clés: dendroctone du pin ponderosa, classification du bois, pourriture, aubier, spectroscopie visible/proche infrarouge (NIR)

Table of Contents

Abstract	iii
Table of Contents	iv
List of Tables	iv
List of Figures	v
1 Introduction	1
2 Methods	2
2.1 Stationary Lumber	2
2.1.1 Paprican chip sensor	3
2.1.2 Additional ASD visible/NIR spectra and colour coordinates	5
2.2 Moving Lumber	5
3 Results and Discussion	6
3.1 Stationary Lumber	6
3.1.1 Paprican chip sensor	6
3.1.2 ASD visible/NIR spectra and colour coordinates	14
3.2 Moving Lumber	18
3.2.1 Low speed	18
3.2.2 Higher speeds	26
4 Conclusions	27
5 Acknowledgements	27
6 Contact	27
7 Literature Cited	28

List of Tables

Table 1. Ratings for extent of decay (AWPA E7).	2
Table 2. Average decay ratings and incidence classifications.	5
Table 3. Decay type classifications for moving spectra data set.	6
Table 4. Prediction statistics for PLS-DA 2 class decay classification models.	9
Table 5. Prediction Statistics for PLS-DA decay Type Classification Models.	12
Table 6. Prediction statistics for PLS-DA decay classification models from lumber sides.	14
Table 7. Prediction statistics for PLS-DA models developed using ASD visible/NIR spectra.	15
Table 8. Prediction statistics for PLS-DA models developed excluding red heart using ASD visible/NIR spectra.	18
Table 9. Prediction statistics for PLS models from spectra obtained from moving lumber.	19
Table 10. Prediction statistics for PLS models from spectra obtained from moving lumber.	21
Table 11. Prediction statistics for lumber-grade models from spectra obtained from moving lumber.	25
Table 12. Spectra obtained from moving lumber.	26

List of Figures

Figure 1.	Photographs of decay in lodgepole pine lumber. (A) Sound. (B) Brown rot. (C) Firm red heart. (D) White speck on red heart.....	3
Figure 2.	Photograph of visible/NIR beam collecting a spectrum from lumber.....	4
Figure 3.	Frequency of decay ratings for the overall data set.....	6
Figure 4.	Frequency of decay types in the overall data set.....	7
Figure 5.	Spectra obtained from sides and top/bottom lumber faces.....	8
Figure 6.	Scores plot for principal component analysis of all spectral data.....	8
Figure 7.	Scores plot for partial least squares discriminant analysis of top and bottom spectral data with three decay classes (Model 2).....	10
Figure 8.	Loadings plot for partial least squares discriminant analysis of top and bottom spectral data with three decay classes (Model 2).....	10
Figure 9.	Scores plot for partial least squares discriminant analysis of top and bottom second derivative spectral data with two decay classes (Model 3).....	11
Figure 10.	Loadings plot for partial least squares discriminant analysis of top and bottom second derivative spectral data with two decay classes (Model 3).....	11
Figure 11.	Scores plot for partial least squares discriminant analysis of top and bottom second derivative spectral data with five decay type classes (Model 7).....	13
Figure 12.	Loadings plot for partial least squares discriminant analysis of top and bottom second derivative spectral data with five decay type classes (Model 7).....	13
Figure 13.	Averaged ASD visible/NIR spectra.....	15
Figure 14.	Scores plot for partial least squares discriminant analysis of second derivative spectral data with four decay types (Model 15).....	16
Figure 15.	Loadings plot for partial least squares discriminant analysis of second derivative spectral data with four decay types (Model 15).....	16
Figure 16.	Scores plot for partial least squares discriminant analysis of L*a*b* data with four decay types (Model 18).....	17
Figure 17.	Loadings for partial least squares discriminant analysis of L*a*b* data with four decay types (Model 18).....	17
Figure 18.	Spectra obtained from moving lumber (sound and decayed).....	19
Figure 19.	Predicted average decay rating vs. average decay rating (Model 24).....	20
Figure 20.	Predicted decay incidence vs. decay incidence (Model 28).....	20
Figure 21.	Scores plot from PLS-DA of decay class using second-derivative spectra obtained from moving lumber (Model 34).....	22
Figure 22.	Loadings plot from PLS-DA of decay class using second-derivative spectra obtained from moving lumber (Model 34).....	22
Figure 23.	Scores plot from PLS-DA of incidence class using second-derivative spectra obtained from moving lumber (Model 37).....	23
Figure 24.	Loadings plot from PLS-DA of incidence class using second-derivative spectra obtained from moving lumber (Model 37).....	23
Figure 25.	Scores plot from PLS-DA of decay class using second-derivative spectra obtained from moving lumber (Model 39).....	24
Figure 26.	Loadings plot from PLS-DA of decay class using second-derivative spectra obtained from moving lumber (Model 39).....	24
Figure 27.	Scores plot from PLS-DA of grading data using second-derivative spectra obtained from moving lumber (Model 38).....	25
Figure 28.	Loadings plot from PLS-DA of grading data using second-derivative spectra obtained from moving lumber (Model 38).....	26

1 Introduction

As mountain pine beetle (MPB)-attacked trees age in the forest, the incidence of decay will increase and the type of decay found in the resource is likely to change. In addition to the endemic levels of incipient decay associated with butt rot and red heart, infection with sap-rot fungi will become more prevalent (Kim et al. 2005). Lewis et al. (2006) reported that the incidence of sap-rot in MPB-attacked trees increased with time since death; given the inability of harvesting to keep up with the current epidemic, sawmills can expect to process increasing amounts of sap-rot in post-MPB wood.

While not readily visible to the naked eye in its early (incipient) stage, as it develops, decay appears as discoloured wood and eventually pockets of rot. In the normal process of grading lumber, a grader visually inspects the lumber and places visibly decayed lumber into lower grades. However, the speed at which lumber is produced from a typical modern planer mill and the fact that the sapwood is already discoloured from blue stain makes it more difficult for graders to visibly detect decay other than advanced pocket rot or similar defects in post-MPB lumber. Furthermore, the increased incidence of decay may make it difficult for graders to keep on top of this defect.

Frequently, modern grading first involves on-line measurement of lumber stiffness (modulus of elasticity) or X-ray measurement of density, which is used to estimate mechanical properties, and is followed up with visual grading. Among other things, visual grading evaluates the presence of unsound wood, white speck and honeycomb in light framing dimension lumber (National Lumber Grades Authority (NLGA) 2003). Unsound wood is a catch-all group for decay that includes white speck, honeycomb and brown rot. White speck is a specific type of decay that causes small white or brown pits or spots in the wood. Honeycomb is similar to white speck, but has larger pits. A 5.1 cm thick “#2” board cannot have more than 1/6th of the width covered by honeycomb, or 1/12th the width covered by unsound wood no longer than 5.1 cm, or firm white speck covering more than 1/3 of the face (NLGA 2003). A 5.1 cm thick “utility” board cannot have more than 1/3rd of the cross section containing unsound wood at any point along the length and must have the nailing edge intact. White speck and honeycomb must be firm (NLGA 2003). Visual grading can be accomplished by human eye or using automated grading systems. These systems are based on colour cameras and have been found to do a reasonably good job of detecting several visual defects including forms of decay (McDonald 2008). In post-MPB lumber, one such system was able to detect 80%-89% of the honeycomb, 70%-79% of the white speck, and 60%-69% of the unsound wood (McDonald 2008).

Visible and near infrared (NIR) spectroscopy measure the intensity of light transmitted by or reflected from a sample from 380 to 800 nm and 800 to 2500 nm, respectively. The visible region is sensitive to electronic transitions in transition metals and highly conjugated organic compounds, while the NIR region is sensitive to vibrational energy changes, particularly O-H and N-H stretching and vibrational overtones from the mid-infrared region.

Visible/NIR spectra from wood contain a wealth of spectroscopic information, but are often difficult to interpret because there are few well defined peaks. The use of multivariate statistical methods to analyse these data has made NIR more accessible. Principal Component Analysis (PCA) is used to simplify and interpret large or complex data sets. The first Principal Component (PC) is calculated to determine the major axis of variation in the spectral data set. The second PC represents the second greatest variation in the data set that is orthogonal to the first PC and so on. PCA is interpreted by looking at scores plots, which provide a graphical representation of where samples lie relative to the principal components. Scores plots can be used to look for groups, trends, outliers or similarities between samples (Eriksson et al. 2006). The degree to which specific wavelengths influence a model is determined by spectral loadings. Highly negative and highly positive loadings both have large impacts on the model. Partial Least Squares (PLS) and Partial Least Squares Discriminant Analysis (PLS-DA) correlate variations in the spectral data set with variations in an external data set (i.e. decay ratings). PLS is used to make quantitative predictions from spectral data. PLS-DA is used to classify samples based on spectral data.

NIR spectroscopy, in combination with multivariate statistical modeling, is capable of rapidly estimating a wide variety of wood properties, including decay. Several researchers have used NIR to classify types of decay (Fackler et al. 2007) or quantify extent of decay (Hoffmeyer and Pedersen 1995; Kelley et al. 2002). For the pulp and paper sector, lab-scale models have been developed to estimate the extent of decay, as indicated by 1% caustic solubility and buffering capacity, in lodgepole pine (Stirling et al. 2007). Research at FPInnovations – Paprican Division has developed NIR models for moisture content, density, brightness, and decay on solid wood cores and over moving conveyers of wood chips (Hsieh et al. 2006). These models have a high degree of accuracy and are amenable to automation. The present research aimed to extend this technology to detect decay in lumber and to determine whether spectral information from the near infrared region could improve existing technology which relies upon information from the visible region. During the work, it became obvious that the scan area was too wide (8 cm) so a hand-held NIR instrument was used to scan smaller areas. Furthermore, the data suggested that the visible part of the spectrum was the most important, so a hand-held visible light spectrophotometer was used to determine if this simpler technology might prove equally effective.

In this study we evaluated the use of near infrared (NIR) spectroscopy to identify decay in post-MPB lumber.

2 Methods

2.1 Stationary Lumber

Fifty-six kiln-dried post-MPB lodgepole pine 2.4 m two-by-fours, selected because they contained significant amounts of decay, were obtained from Canfor Polar Division. All boards were graded #2 or utility by the mill. Each board was given a unique identifier, and each face was divided into approximately 10 cm sections for a total of 4303 sections. The bark side of each board was labelled *top* and the pith side labelled *bottom*. Holes were avoided since they can already be easily detected and because they would greatly influence spectra. Lumber markings were also avoided since scanning in a mill would occur before marking. Bark and knots were included as these were considered natural variations that any model would have to be able to handle. Each section was rated for decay (Table 1) based on the criteria outlined in American Wood Protection Association (AWPA) standard E7-07 (AWPA 2008) and for type of decay (Figure 1). Decay type classifications were sound, brown rot, white speck, red heart and non-decay characteristics. A few samples of honeycomb were identified and included with white speck. Most white speck samples occurred on wood that also had red heart. The non-decay characteristics group was included as a catch-all group for sound wood with blue stain, resin pockets, beetle holes, large knots or pith.

Table 1. Ratings for extent of decay (AWPA E7-07).

Rating	Description
10	Sound
9.5	Suspicion of decay
9	Trace decay (up to 3% cross-section)
8	Decay (3 – 10% cross-section)
7	Decay (10 – 30% cross-section)
6	Decay (30 – 50% cross-section)
4	Decay (50 – 75% cross-section)
0	Failure

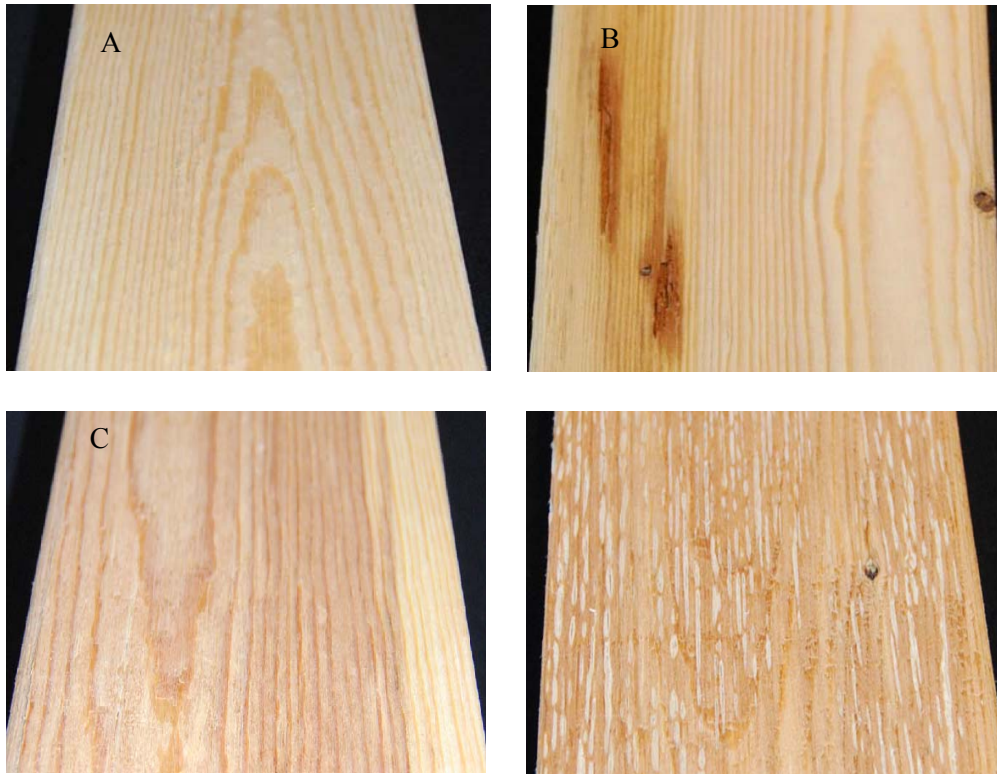


Figure 1. Photographs of decay in lodgepole pine lumber. (A) Sound. (B) Brown rot. (C) Firm red heart. (D) White speck on red heart.

2.1.1 Paprican chip sensor

Each decay-rated section was scanned using the Paprican chip sensor. This is a visible/NIR spectrometer developed by FPInnovations – Paprican for monitoring chip quality attributes in real time that collects spectra from 300 to 1700 nm. A self-contained diffuse reflectance probe head with an 8 cm elliptical spot size aligned with the length of the board (developed for the Paprican sensor) was placed approximately 1 m above the sample and reflected light returned to the spectrometer via fibre optic cables. For each sample, 100 scans each lasting 25 μ s were averaged into the final spectrum used in modelling. Before scanning, the source lamp was given 5 min to warm up. Instrument set-up is shown in Figure 2.

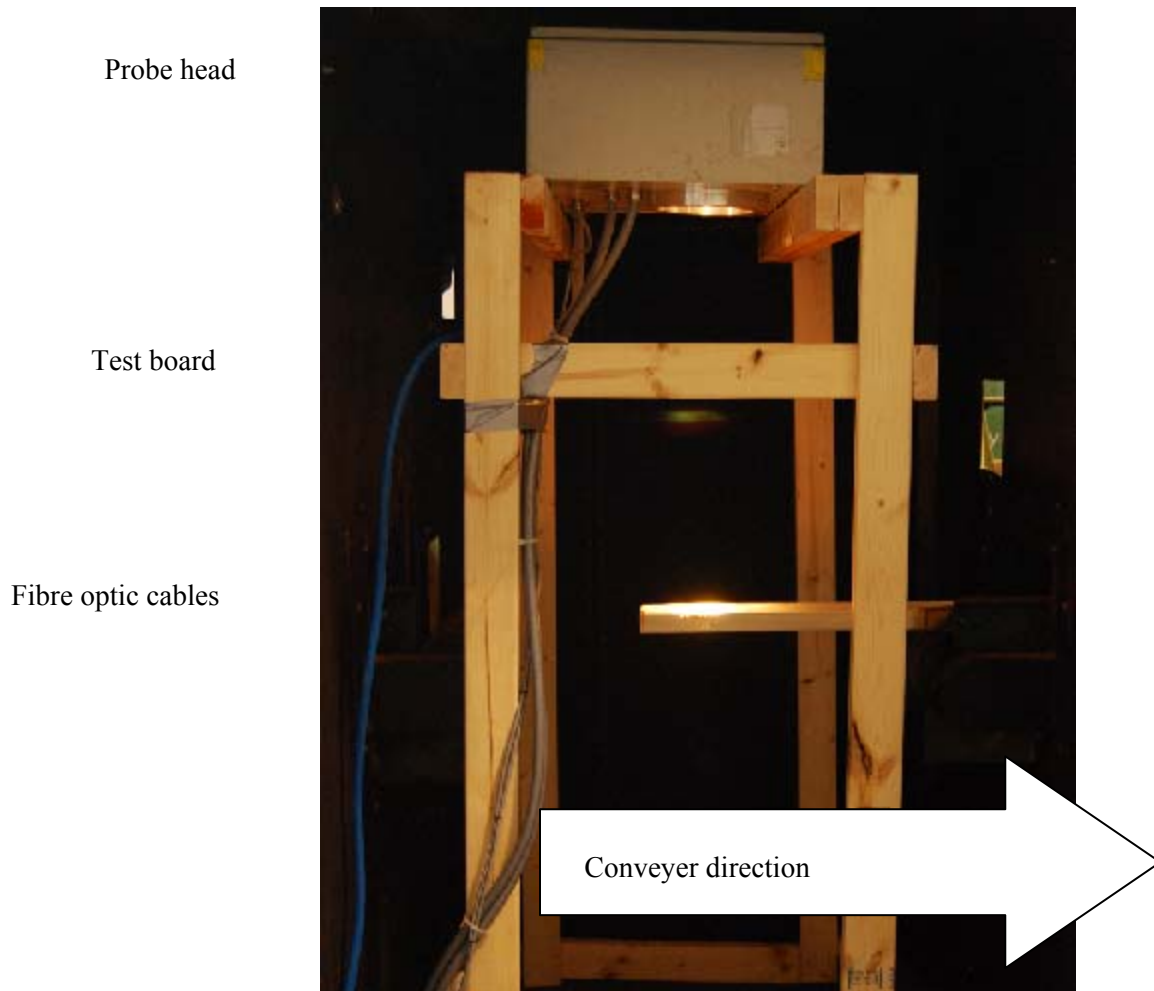


Figure 2. Photograph of visible/NIR beam collecting a spectrum from lumber.

Spectra were sorted in Grams AI version 9.0 (ThermoFisher Scientific, Philadelphia, PA) and aligned with decay ratings. Spectral and ratings data were imported into Simca-P version 11 (Umetrics, Umeå, Sweden) for chemometric analysis. A PCA was performed on all of the spectral data to gain some insight into the underlying pattern. Based on this analysis, the overall data set was separated into spectra obtained from the top or bottom of the lumber (the larger faces), and spectra obtained from the sides (the smaller faces). Both of these data sets were further divided into two data sets: calibration and validation. The calibration data sets were used to construct PLS-DA models that used spectral data to further classify decay-rated sections based on level or type of decay. The validation data sets were excluded from model development and used to evaluate the performance of the models. Mean centering, unit variance and Pareto scaling of the spectra, Multiplicative Signal Correction (MSC), Standard Normal Variate (SNV) correction, first- and second-order derivation, and logarithmic scaling of spectral and ratings data were investigated for their ability to improve decay and defect classification. First- and second-order derivatives were prepared from 7-point Savitzky-Golay algorithms (Savitzky and Golay 1964). Models were evaluated based on Q^2 (cumulative), which represents the proportion of variation that can be accounted for by the model (Eriksson et al. 2006), and by their ability to accurately classify or quantify decay extent and type in an external data set.

2.1.2 Additional ASD visible/NIR spectra and colour coordinates

Selected spots from all sides were scanned using an ASD Labspec 5000 (ASD, Boulder, CO). The spectrometer collects spectra over a wider range (350 to 2500 nm) but has a slower spectral acquisition time (100 ms) than the Paprican chip sensor. The probe head has a smaller spot size (2 cm diameter) and touches the wood. One hundred and eighty spots were selected from 20 boards. These included 60 sound, 60 brown rot, 30 firm red heart and 30 white speck samples (in most of the samples white speck occurred on wood containing red heart). A Spectralon™ reference baseline was scanned every 30 min during spectral collection. Colour coordinates (L*a*b*) were also obtained on these samples using a Minolta CM700d spectrophotometer. PLS-DA models were prepared from these data as described above.

2.2 Moving Lumber

Visible/NIR spectra were obtained using the Paprican chip sensor from the top and bottom faces of the 56 pieces of lumber described above while moving along a conveyer at 61 m/min (200 fpm). Twenty-seven to twenty-nine spectra were obtained from each face. When the scan collection time included air, before or after the lumber moved under the spectrometer, spectra were clearly distorted. These spectra were removed based on their appearance. The remaining spectra were averaged to provide two spectra for each board (top and bottom). The overall data set contained 112 spectra but was divided into a calibration data set containing 84 spectra and an external validation data set containing 28 spectra.

Ratings of decay for each board, top and bottom, were averaged to provide an overall decay rating for the face. In addition, the number of ratings of 9.5 or less for each board face was determined to provide a measure of decay incidence for each board. Average decay ratings and decay incidence were used to construct PLS models. Based on the average decay ratings and decay incidence, three decay classes were defined as shown in Table 2. These classifications were used to develop PLS-DA models. Average decay type ratings were placed into five classes and modeled using PLS-DA (Table 3).

PLS-DA models were also prepared to predict the lumber grade from averaged top and bottom spectra. Two class models were used since this data set contained only utility and #2 grades.

In addition, spectra were collected over lumber moving at speeds from 61 to 244 m/min to determine the effects on spectral quality.

Table 2. Average decay ratings and incidence classifications.

Decay Class	Average Decay Rating	Decay Incidence (# of ratings 9.5 or less)
Clear	10	0
Low decay	9.75 – 9.99	1 – 7
High decay	Less than 9.75	8 or more

Table 3. Decay type classifications for moving spectra data set.

Decay Class	Description
Clear	Clear (2 or fewer ratings of 9.5 or less)
Brown rot	More than 2 ratings of 9.5 or less Brown rot most abundant
Red heart	More than 2 ratings of 9.5 or less Red heart most abundant
White speck	More than 2 ratings of 9.5 or less White speck most abundant
Non-decay characteristics	Two or fewer ratings of 9.5 or less and more than 2 non-decay characteristics, including blue stain, resin pockets, beetle holes and knots and pith

3 Results and Discussion

3.1 Stationary Lumber

3.1.1 Paprican chip sensor

Despite selecting for pieces with decay present, the overall incidence of decay in each 10 cm segment on each face of the board was low. Eighty-two percent of the evaluated segments were rated 10 (sound). This posed a challenge for modeling since the decayed segments were under-represented. Nevertheless, the total number of samples was large, including the number of decayed samples, and even higher proportions of sound lumber would likely be found in sawmills. Similarly, brown rot, red heart and white speck were found in significant quantities but were much less frequent than sound wood (Figure 4). Brown rot frequently occurred in small pockets (5-10 cm) while red heart and white speck tended to cover much larger areas. Non-decay characteristics including resin pockets, blue stain, as well as knots and pith and beetle holes were also observed.

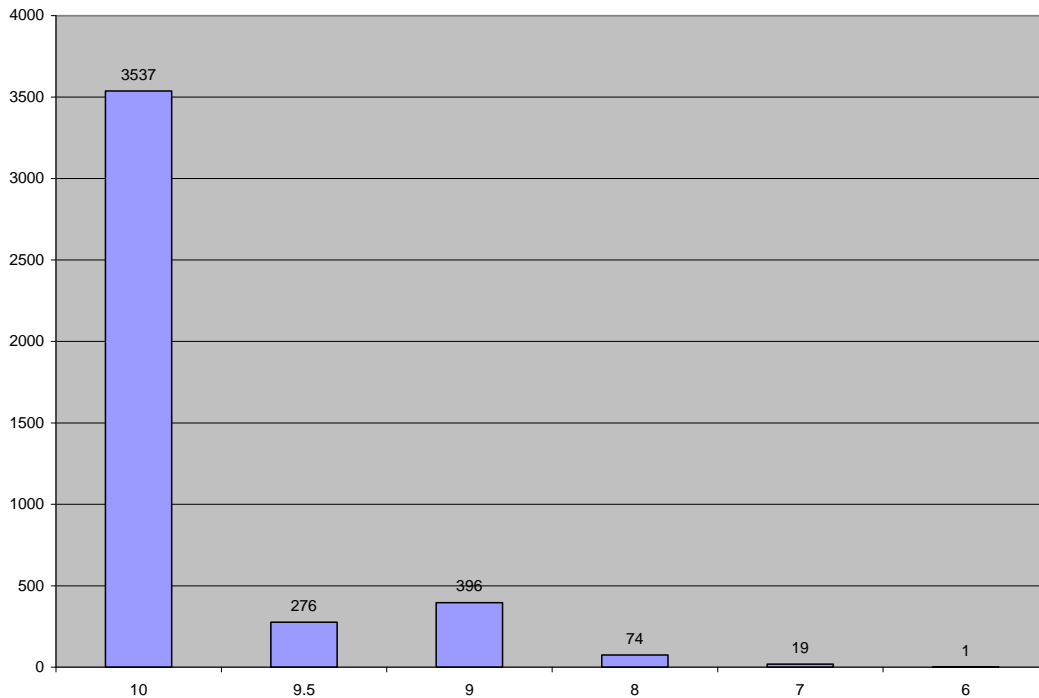


Figure 3. Frequency of Decay Ratings for the Overall Data Set.

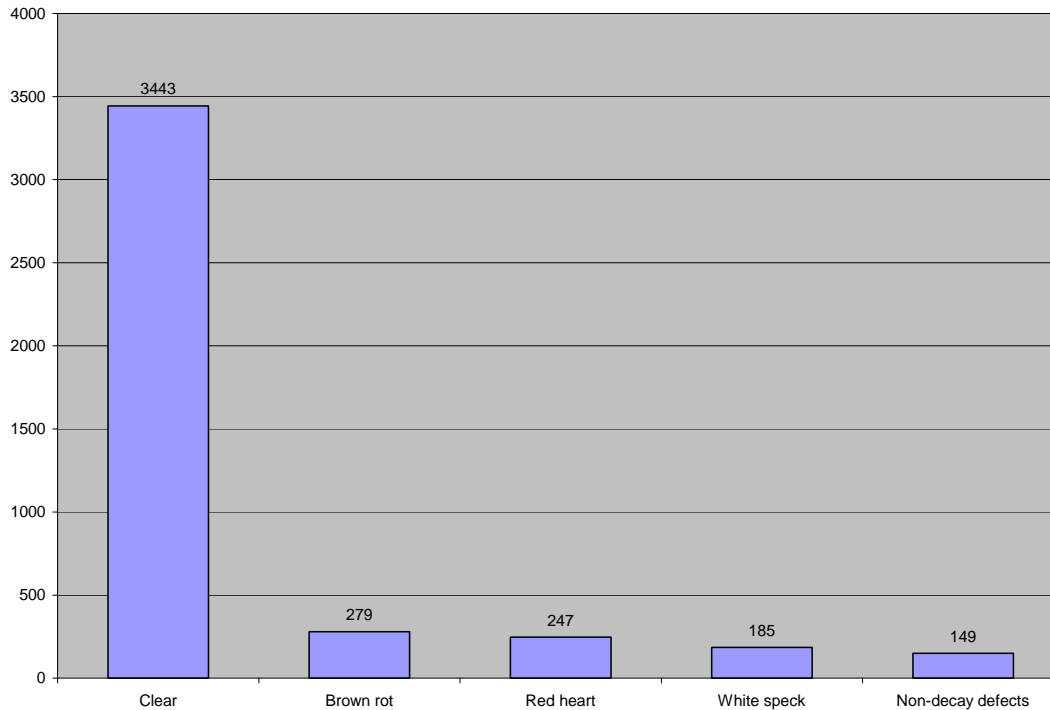


Figure 4. Frequency of decay types in the overall data set.

All spectra had a similar shape (Figure 5). As is common in NIR spectroscopy, there were no distinct peaks that could be measured and correlated with variables of interest (in this case, decay). Multivariate statistical methods were thus needed to determine whether these spectra could be used to identify decayed lumber. The spectra shown in Figure 5 are not offset. The spectra obtained from the sides of the lumber had higher absorbance than spectra obtained from the top or bottom of the boards. As a result of these major spectral differences, the principal component analysis of all the spectral data separated spectra based on whether they were obtained from the top/bottom or sides of the boards (Figure 6). One way of removing the effect of baseline is by using derivative spectra. This did result in more similar-looking spectra, but PCA still clustered spectra based on whether the spectra were obtained from the top/bottom or sides of the boards. These differences are likely due to the change in position of the board with respect to the spectrometer. Based on these differences, it was decided to model spectra obtained from the top and bottom faces separately from spectra obtained on the sides of the lumber. Figure 5 also shows a slight separation of top and bottom spectra. This is likely due to the greater prevalence of sapwood on the top of the boards and heartwood on the bottom.

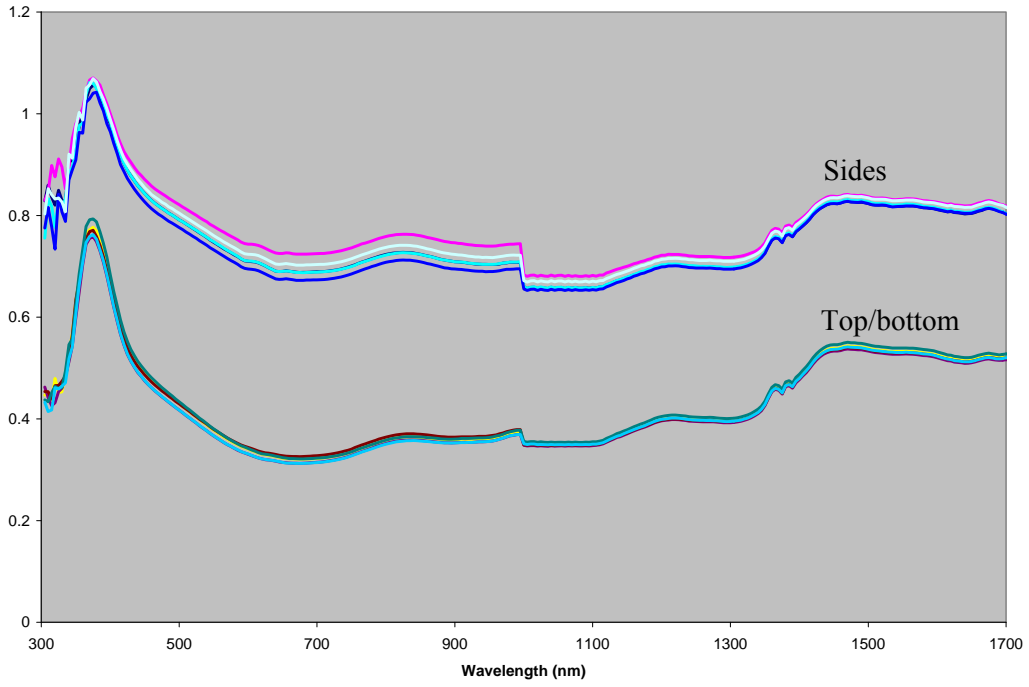


Figure 5. Spectra obtained from sides and top/bottom lumber faces.

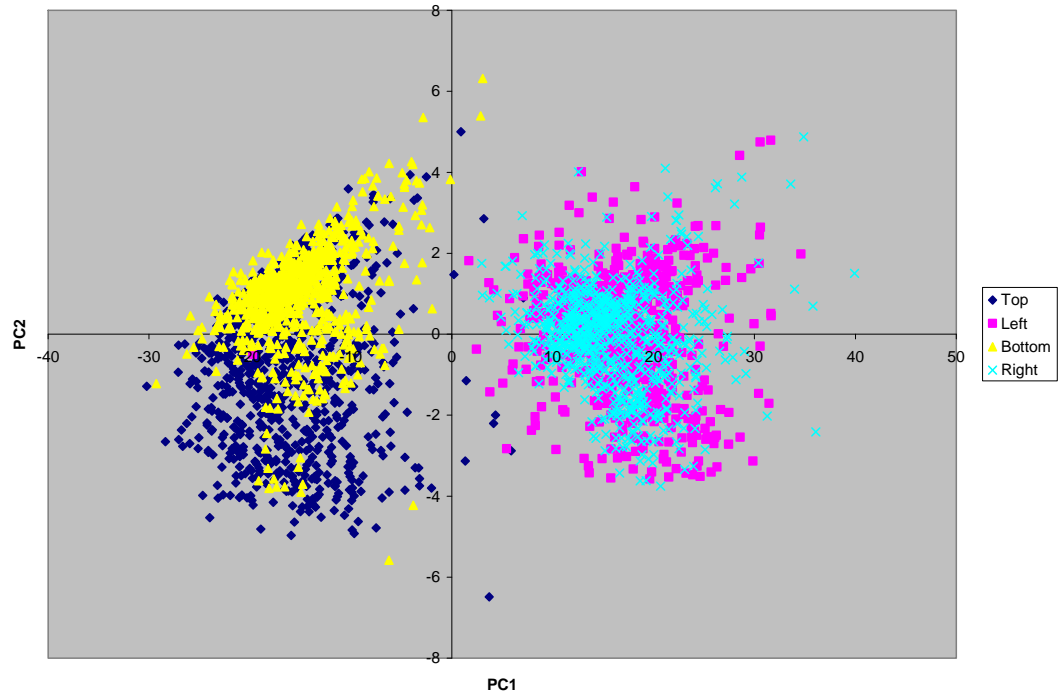


Figure 6. Scores plot for Principal Component Analysis of all spectral data.

3.1.1.1 Modeling spectra from the top and bottom faces

Spectra from the tops and bottoms of boards all had a similar shape. There were few distinct differences between clear and decayed samples. An initial PCA of spectral data showed no separation corresponding to decay. Only two samples stood out as potential outliers in this PCA and in subsequent PLS-DA models (Figure 7). Both of these spectra were associated with large bark pockets. Their removal did not improve the identification of decayed wood, so for completeness they were retained throughout.

PLS-DA was used to develop models to classify samples based on decay ratings from their spectra. Table 4 lists the best-developed models. The high overall classification accuracy of all of the models reflects the high proportion of sound wood in the data set. The first basic PLS-DA model (Table 4, Model 1) classified samples as sound (rated 10) or decayed (rated 9.5 or less). The second model was the same but used three classification categories (10, 9.5, and 9 or less). Neither of these models was able to classify decay accurately, but the distribution of samples rated 9.5 was shown to more closely match those rated 9 or less (Figure 7). As a result, the remaining classification models were based on two classes. The loadings from these models were greatest in the visible region (400-700 nm), so this region was selected for future modeling (Figure 8).

Second derivative spectra were found to improve the predictive ability of the models (Model 3, Table 4). The scores plot obtained using second derivative spectra (Figure 9) shows greater separation of sound and decayed wood, but still significant areas of overlap. The loadings from the second derivative spectra (Figure 10) were quite different as slope and baseline effects had been removed; however, they retained a high loading in the visible region.

The loadings from all of the models indicate that the region from 400 to 700 nm has the greatest impact on the models. To try to improve classification, two-class PLS-DA models were developed from 400 to 700 nm (Table 4). Models based on the 400 to 700 nm region were able to achieve roughly the same classification accuracy as the models based on the full spectral range using fewer principal components.

The effect of scaling, transformation and spectral region were all investigated. When derivative spectra were not used, centre scaling produced the best models. When second derivative spectra were used, scaling to unit variance produced the best models. Logarithmic, MSC, SNV and 1st derivative spectral transformations were not found to improve the model accuracy.

Table 4. Prediction statistics for PLS-DA 2 class decay classification models.

Model #	Scaling	Trans.	Region	PCs	Q ²	Overall classification accuracy (n = 515) %	Classification accuracy of samples rated 10 (n = 422) %	Classification accuracy of samples rated 9.5 or less (n = 93) %
1	Centre	None	300-1700	8	0.44	91	99	55
2*	Centre	None	300-1700	8	0.30	83	99	44% for 9.5, 0% for 9 or less
3	Unit variance	2 nd deriv.	300-1700	5	0.47	92	99	61
4	Centre	None	400-700	6	0.45	90	98	54
5	Unit variance	2 nd deriv.	400-700	5	0.46	90	98	51

* 3 class model

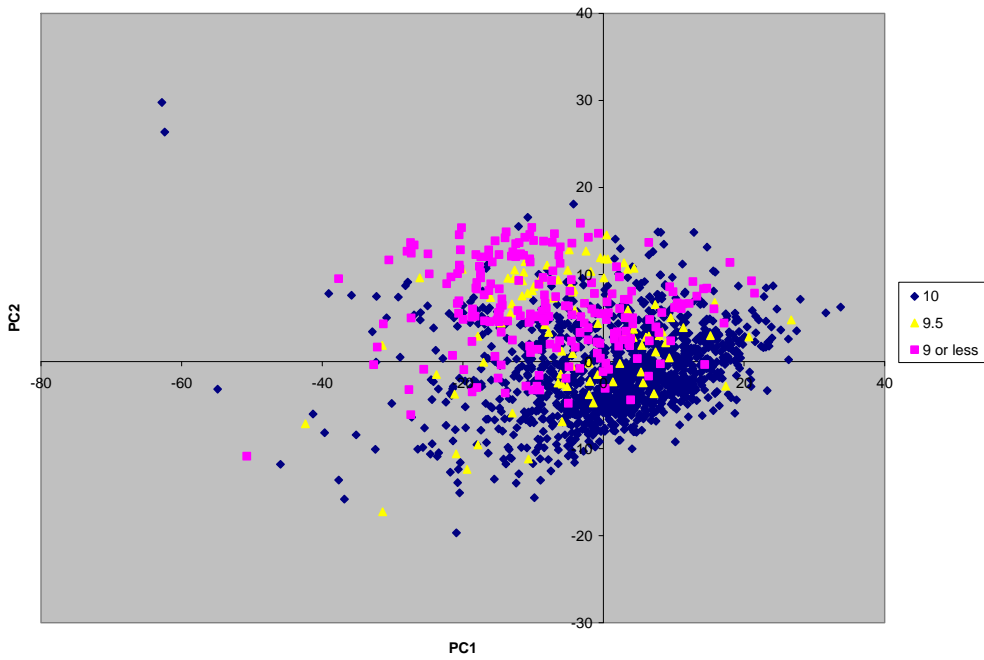


Figure 7. Scores plot for partial least squares discriminant analysis of top and bottom spectral data with three decay classes (Model 2).

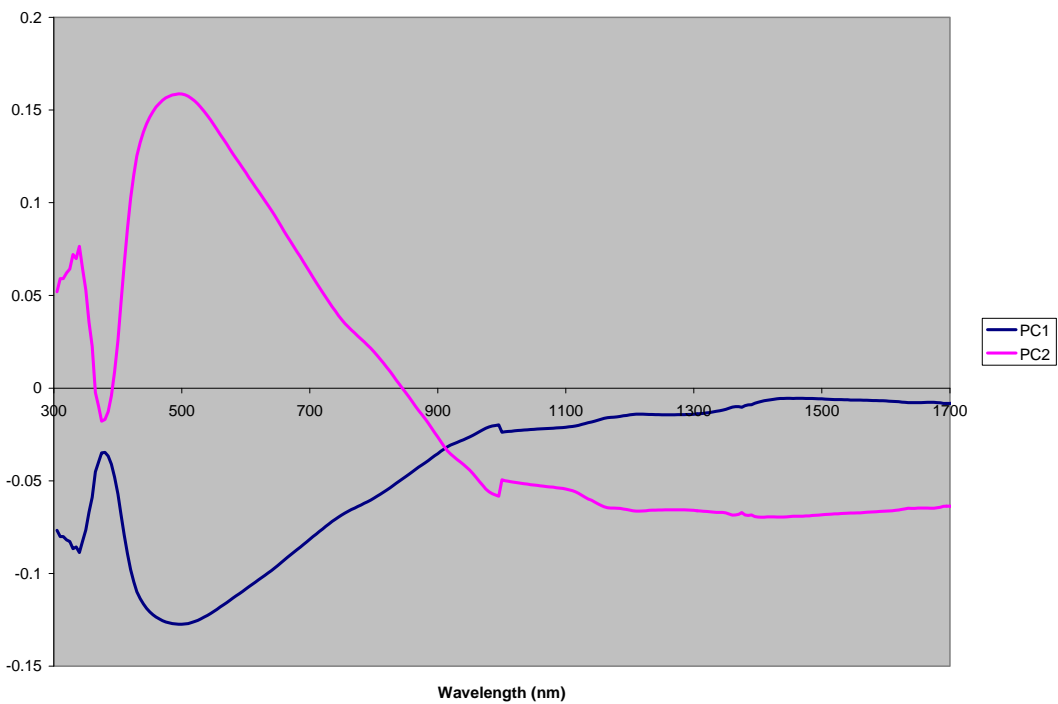


Figure 8. Loadings plot for partial least squares discriminant analysis of top and bottom spectral data with three decay classes (Model 2).

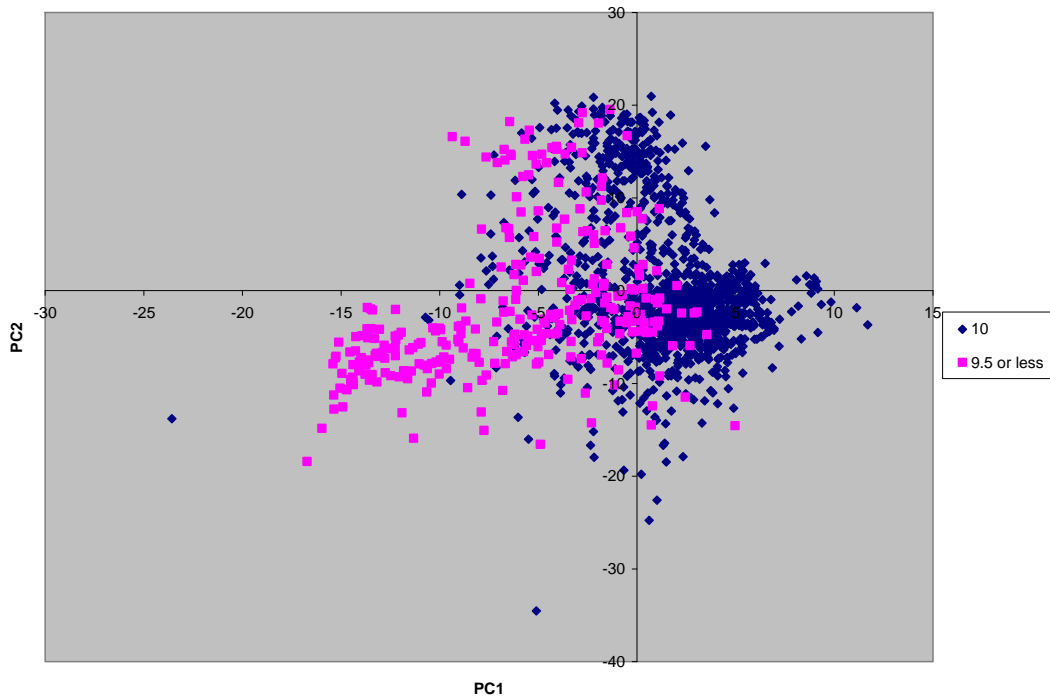


Figure 9. Scores plot for partial least squares discriminant analysis of top and bottom second derivative spectral data with two decay classes (Model 3)

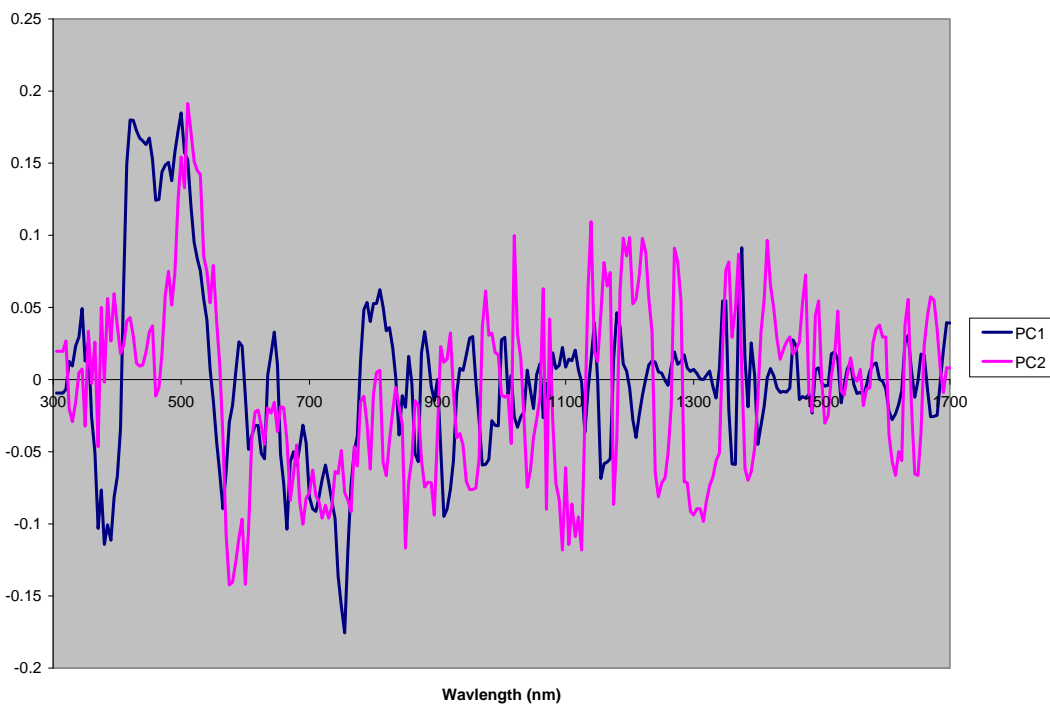


Figure 10. Loadings plot for partial least squares discriminant analysis of top and bottom second derivative spectral data with two decay classes (Model 3).

Samples were also classified based on the type of decay observed. The four models described in Table 5 use normal and second-derivative spectra from the full range and visible range only. The model based on second-derivative spectra over the entire range (Model 7) was best able to classify decay type. Twenty-two of 23 external red heart samples were accurately classified. Some separation of brown rot and white speck from clear wood is evident, though there is a large area of overlap (Figure 11). Red heart is clearly distinguishable from the other defects. No other defects were accurately classified by any of the models. Due to the low incidence of non-decay characteristics, defects within this group (such as blue stain) were not considered independently. Loadings were greatest in the visible region for decay type classification (Figure 12). It therefore fits that red heart, a highly visible characteristic, is accurately identified by the model.

Table 5. Prediction statistics for PLS-DA decay type classification models.

Model #	Scaling	Trans.	Region	PCs	Q ²	Overall classification accuracy (n=515) %	Clear (n=412) %	Brown rot (n=40) %	Red heart (n=23) %	White speck (n=28) %	Non-decay defect (n=12) %
6	Centre	None	300-1700	7	0.25	85	99	18	91	4	0
7	Unit variance	2 nd deriv.	300-1700	8	0.30	87	99	25	96	25	0
8	Centre	None	400-700	5	0.23	85	100	18	96	0	0
9	Unit variance	2 nd deriv.	400-700	3	0.24	86	100	28	96	0	0

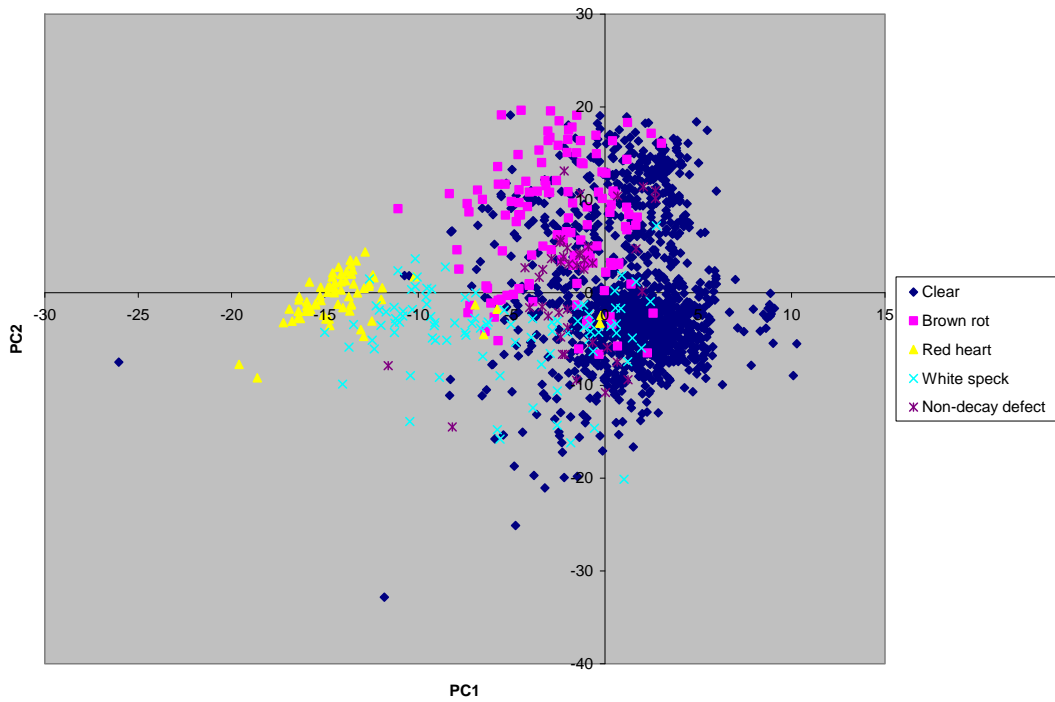


Figure 11. Scores plot for partial least squares discriminant analysis of top and bottom second derivative spectral data with five decay type classes (Model 7).

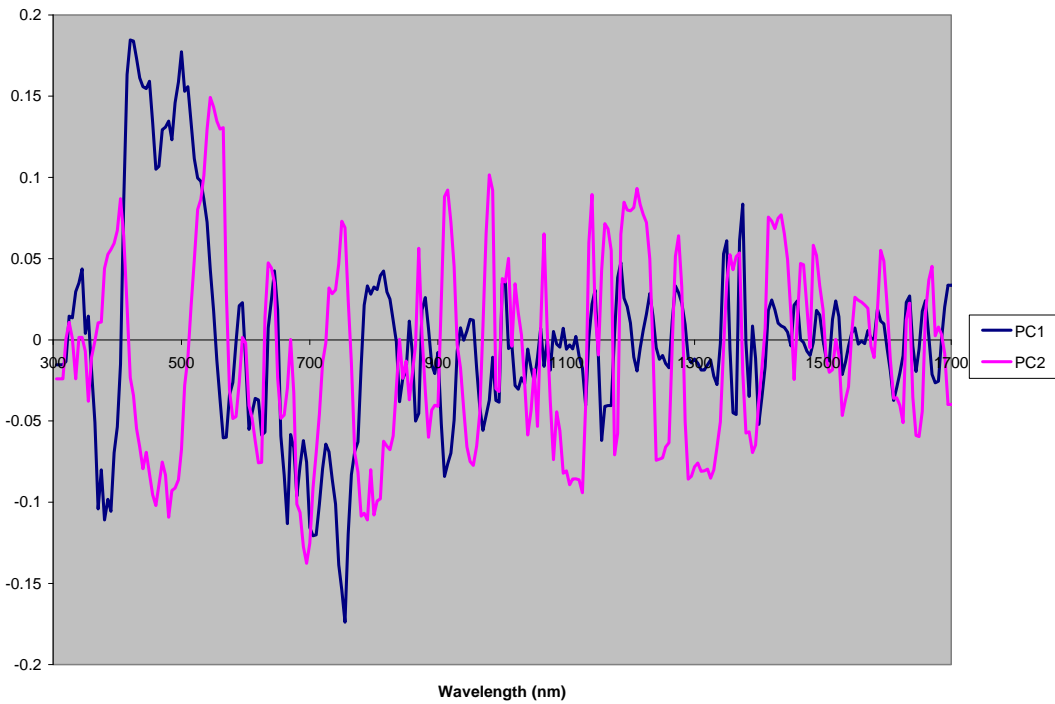


Figure 12. Loadings plot for partial least squares discriminant analysis of top and bottom second derivative spectral data with five decay type classes (Model 7).

3.1.1.2 Modeling spectra from the sides

Two-class PLS-DA models were prepared for spectra obtained from the sides of lumber. Table 6 shows the four models developed. The best model (Model 11) used second-derivative spectra over the entire range. Scores for this model indicated incomplete separation of sound and decayed wood, similar to models based on top and bottom spectra. Loadings again pointed to the importance of the visible region. Although the spectra have a different appearance, models from the top/bottom and models from the sides were very similar in their inability to classify decayed wood.

Table 6. Prediction statistics for PLS-DA decay classification models from lumber sides.

Model #	Scaling	Trans.	Region	PCs	Q ²	Overall classification accuracy (n = 492) %	Classification accuracy of samples rated 10 (n = 405) %	Classification accuracy of samples rated 9.5 or less (n = 87) %
10	Centre	None	300-1700	8	0.295	88	99	37
11	Unit variance	2 nd deriv.	300-1700	5	0.374	91	99	55
12	Centre	None	400-700	7	0.304	87	99	36
13	Unit variance	2 nd deriv.	400-700	3	0.273	87	99	33

3.1.2 ASD visible/NIR spectra and colour coordinates

Spectra obtained from the ASD spectrometer had a similar shape to those obtained from the Paprican chip sensor but covered a wider range of wavelengths (Figure 13).

PLS-DA models were developed using visible/NIR spectra obtained from selected boards that contained sound wood, red heart, white speck or brown rot (Table 7). These boards contained clearly defined regions of decayed wood. The second derivative full-spectrum model (Model 15) provided the highest classification accuracy. One brown rot sample was misclassified as white speck, two white speck samples were misclassified as brown rot and red heart, and three red heart samples were misclassified, one as white speck and two as sound. All sound samples were accurately predicted. The classification of one decay type for another is not as serious an error as the classification of decayed wood as sound, so, practically, the prediction accuracies are higher than those presented in Table 7. The scores plot for this model shows good separation of all decay types (Figure 14). The loadings plot indicates that all regions of the spectra are being used to construct the model (Figure 15).

Spectrophotometric data (L*a*b*) obtained on the same locations as the ASD visible/NIR spectra were used to construct a PLS-DA model to differentiate decay types. This model (Model 18) did an excellent job of separating all decay types except white speck from red heart (Figure 16). However, four of the five misclassified red heart samples were identified as sound, and six of the eight white speck samples were classified as brown rot. These are acceptable errors since the model is mistaking one type of sound wood for another and one type of decay for another. Loadings indicate that all colour coordinates were used to develop the model (Figure 17). The colourimetric data could be used to predict decay type with similar accuracy to the visible/NIR data.

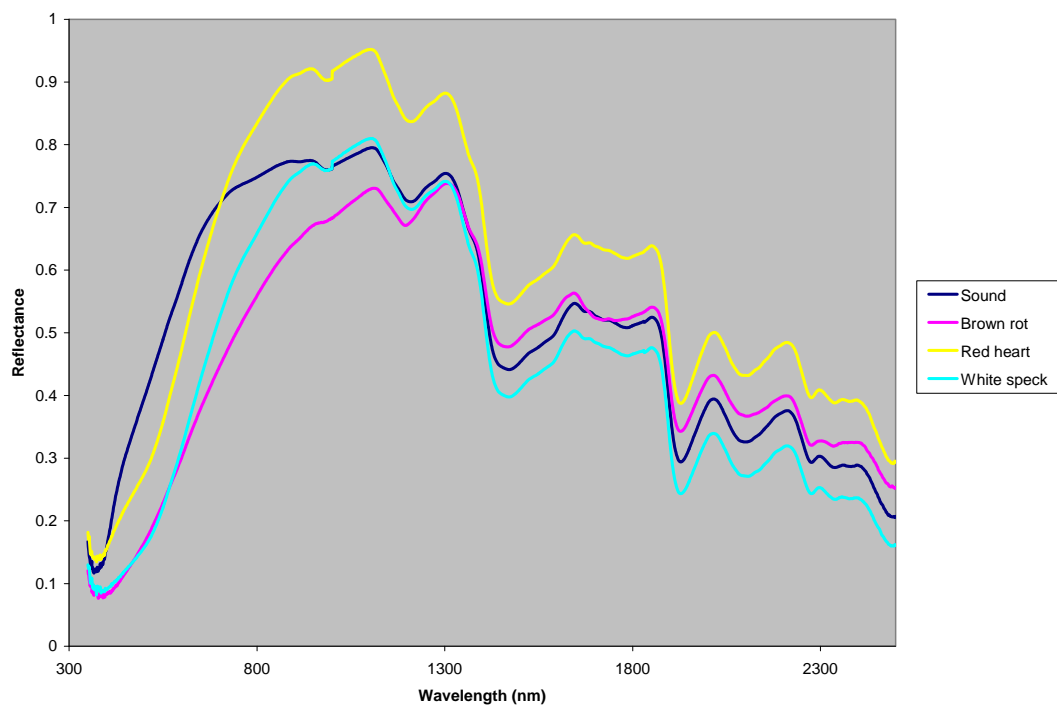


Figure 13. Averaged ASD visible/NIR spectra.

Table 7. Prediction statistics for PLS-DA models developed using ASD visible/NIR spectra.

Model #	Data set	Trans.	Region	PCs	Q ²	Classification accuracy (%)				
						Overall (n=46)	Sound (n=15)	Brown rot (n=15)	Red heart (n=8)	White speck (n=8)
14	Decay type	None	350-2500	10	0.65	83	87	93	88	50
15	Decay type	2 nd deriv.	350-2500	10	0.72	87	93	100	63	75
16	Decay type	None	400-700	8	0.58	70	100	87	50	0
17	Decay type	2 nd deriv.	400-700	7	0.57	72	100	100	38	0
18	L*a*b* Decay type	-	-	2	0.51	67	100	87	38	0

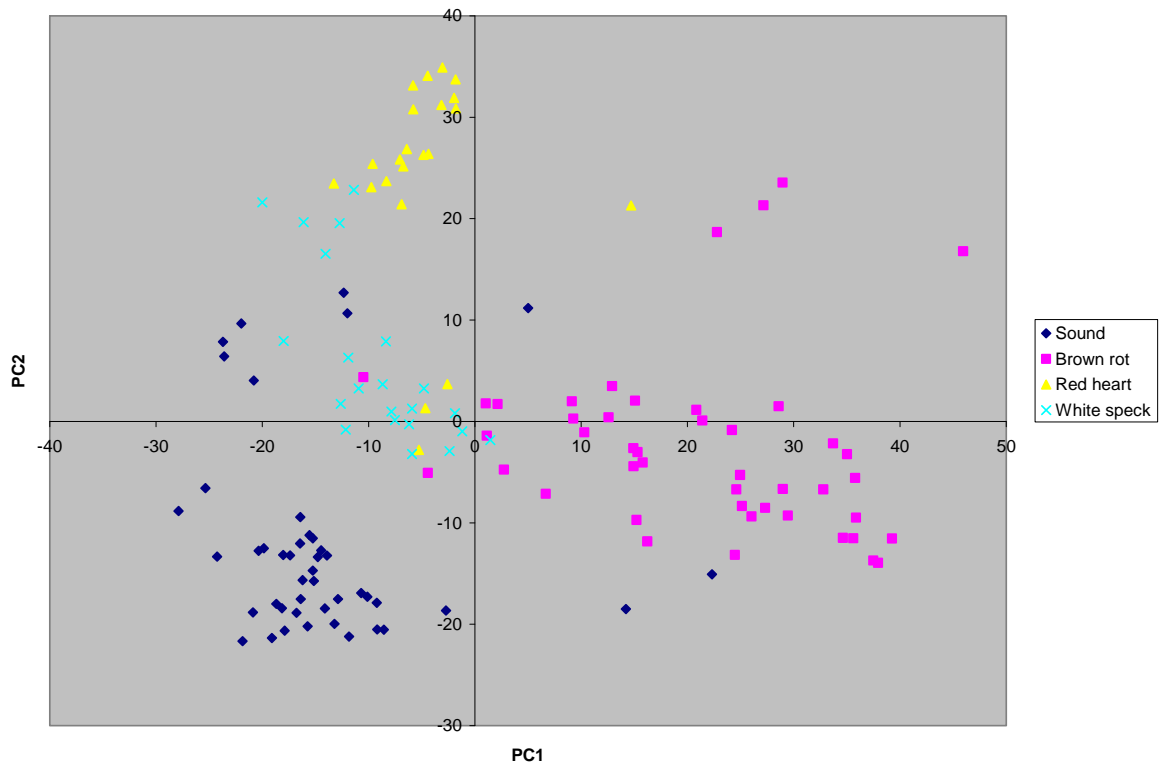


Figure 14. Scores plot for partial least squares discriminant analysis of second derivative spectral data with four decay types (Model 15).

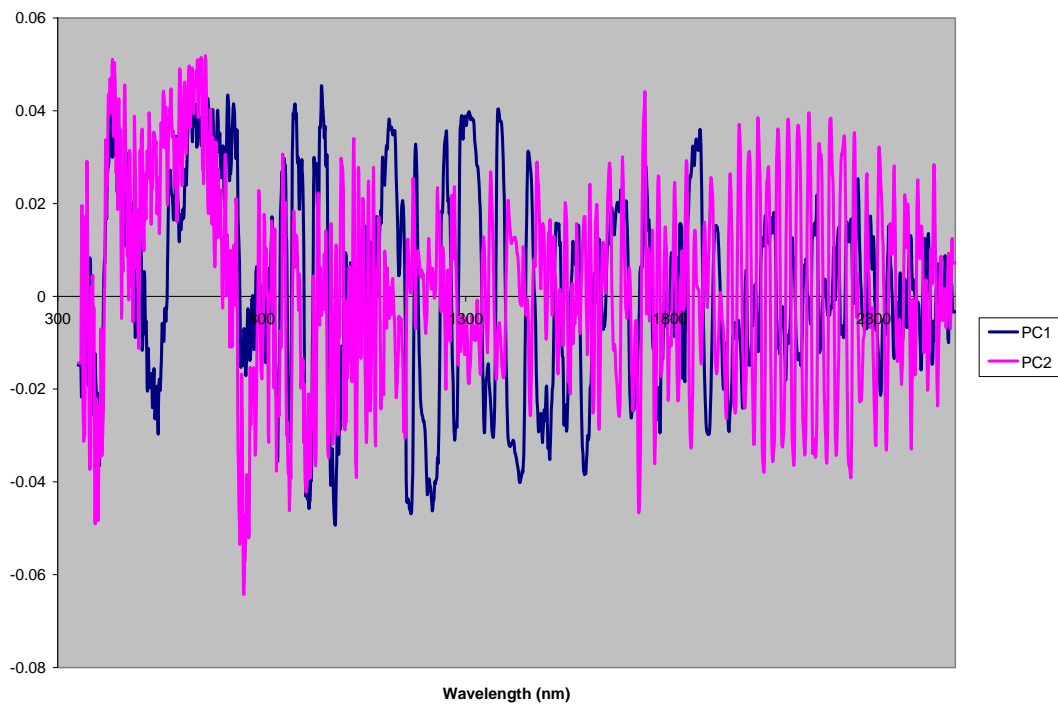


Figure 15. Loadings plot for partial least squares discriminant analysis of second derivative spectral data with four decay types (Model 15).

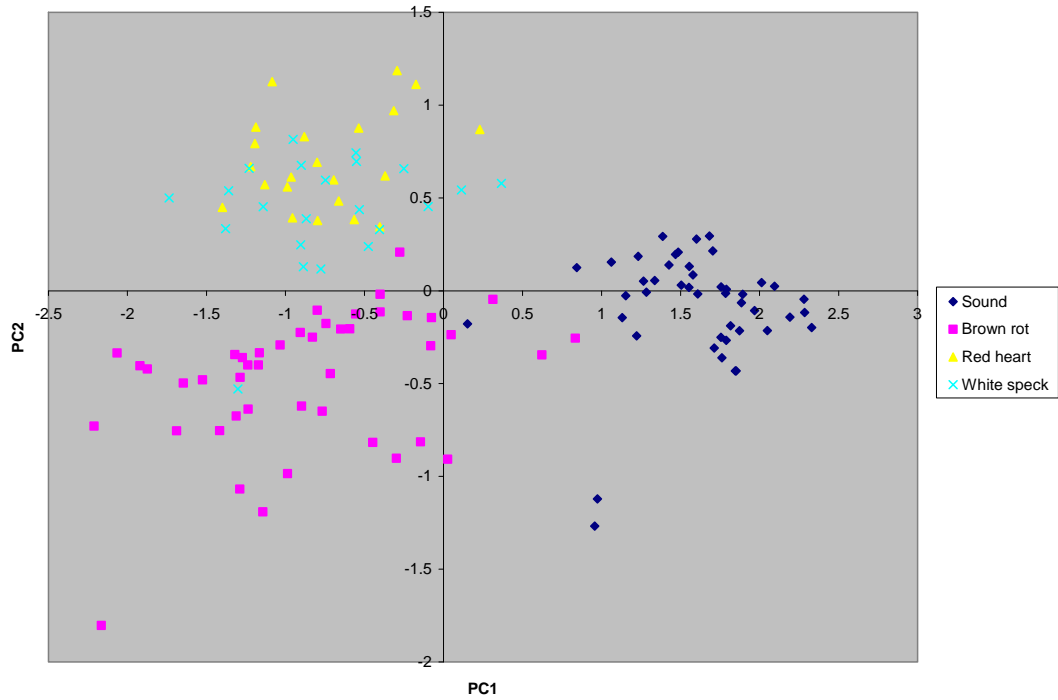


Figure 16. Scores plot for partial least squares discriminant analysis of L*a*b* data with four decay types (Model 18).

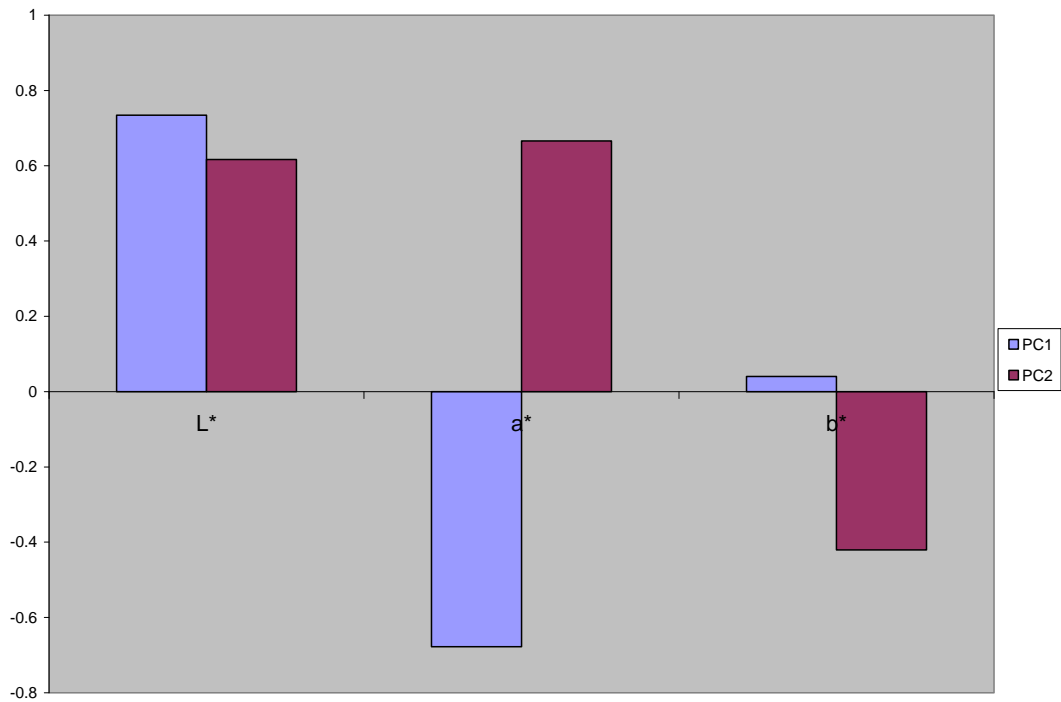


Figure 17. Loadings for partial least squares discriminant analysis of L*a*b* data with four decay types (Model 18).

The L*a*b* scores plot (Figure 16) and, to a lesser extent, the visible/NIR scores plot (Figure 14) indicate poor differentiation of white speck and red heart. This is likely because a light red heart discolouration appears to have a similar redness to a heavy red heart containing white specks. Since red heart is considered to be a minor defect, new models were developed with red heart excluded. These models show the ability to differentiate sound wood, brown rot and white speck (Table 8). Overall, these models are only slightly better than the ones developed including red heart (Table 8). However, Models 19 and 20 do exhibit an improved ability to differentiate white speck from sound wood and brown rot.

Table 8. Prediction statistics for PLS-DA models developed excluding red heart using ASD visible/NIR spectra.

Model #	Data set	Trans.	Region	PCs	Q ²	Classification accuracy (%)			
						Overall (n=38)	Sound (n=15)	Brown rot (n=15)	White speck (n=8)
19	Decay type	None	350-2500	11	0.77	97	100	100	88
20	Decay type	2 nd deriv.	350-2500	8	0.72	97	100	100	88
21	Decay type	None	400-700	9	0.86	89	88	100	63
22	Decay type	2 nd deriv.	400-700	3	0.74	82	100	100	13
23	L*a*b* Decay type	-	-	2	0.66	76	87	73	63

3.2 Moving Lumber

3.2.1 Low speed

Figure 18 shows the average visible/NIR spectra of ten board faces (five clear and five with high levels of decay). The only observable difference between these spectra occurs between 400 and 700 nm, where the spectra from decayed samples have higher reflectance.

The PLS models of average decay and decay incidence both showed a moderate correlation between observed and predicted data (Table 9). In both models, the samples with the lowest and highest levels of decay were most accurately predicted. Samples with a medium amount of decay were predicted to be less decayed than they were (Figures 19 and 20). This indicates that the models lack sensitivity, but are able to identify boards with extensive decay.

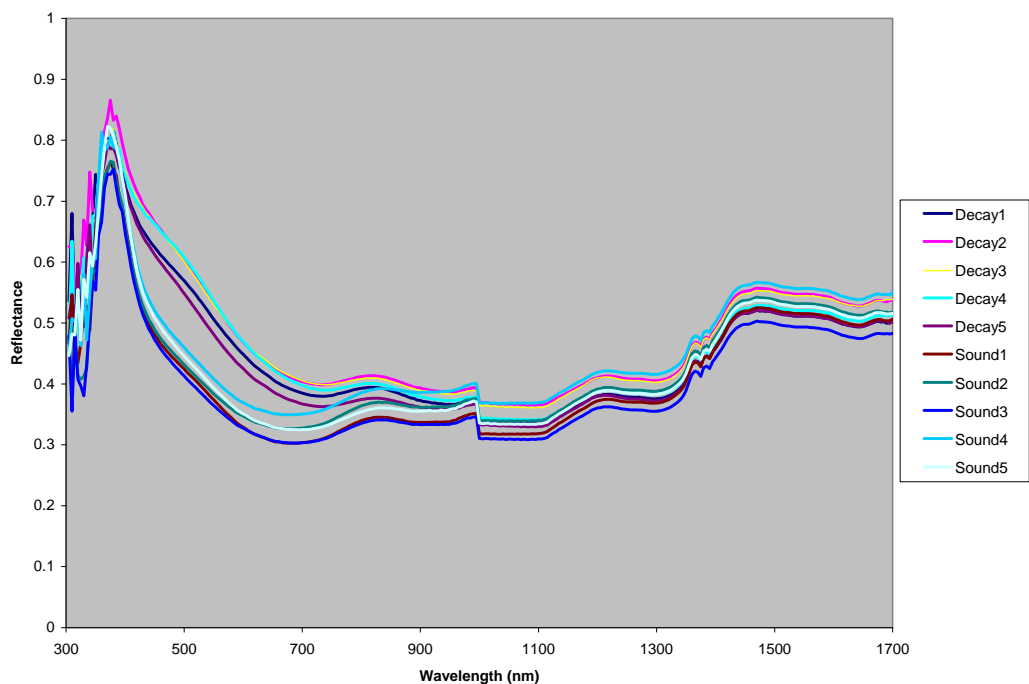


Figure 18. Spectra obtained from moving lumber (sound and decayed).

Table 9. Prediction statistics for PLS models from spectra obtained from moving lumber.

Model #	Rating	Scaling	Trans.	Region	PCs	Q ²	RMSEE	RMSEP
24	Average decay	Centre	None	300-1700	3	0.40	0.20	0.28
25	Average decay	Centre	None	400-700	3	0.43	0.19	0.32
26	Average decay	UV	2 nd deriv.	300-1700	2	0.42	0.17	0.29
27	Average decay	UV	2 nd deriv.	400-700	2	0.49	0.18	0.30
28	Incidence	Centre	None	300-1700	4	0.46	3.7	4.5
29	Incidence	Centre	None	400-700	3	0.52	3.9	4.7
30	Incidence	UV	2 nd deriv.	300-1700	2	0.38	3.4	5.0
31	Incidence	UV	2 nd deriv.	400-700	2	0.52	3.7	4.5

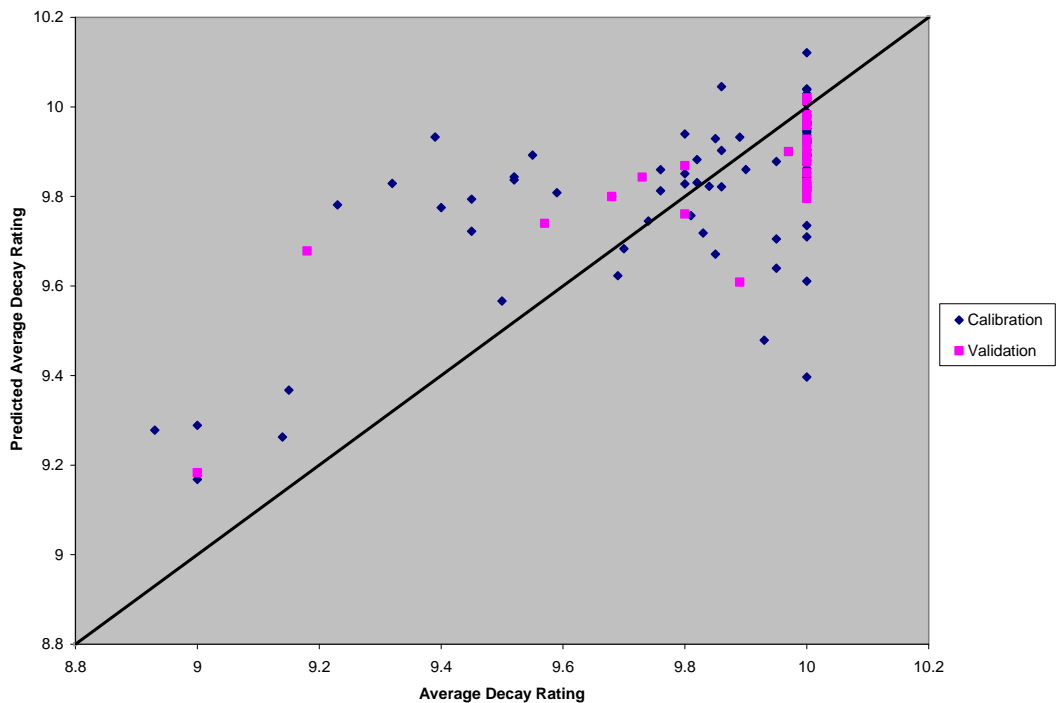


Figure 19 Predicted average decay rating vs. average decay rating (Model 24).

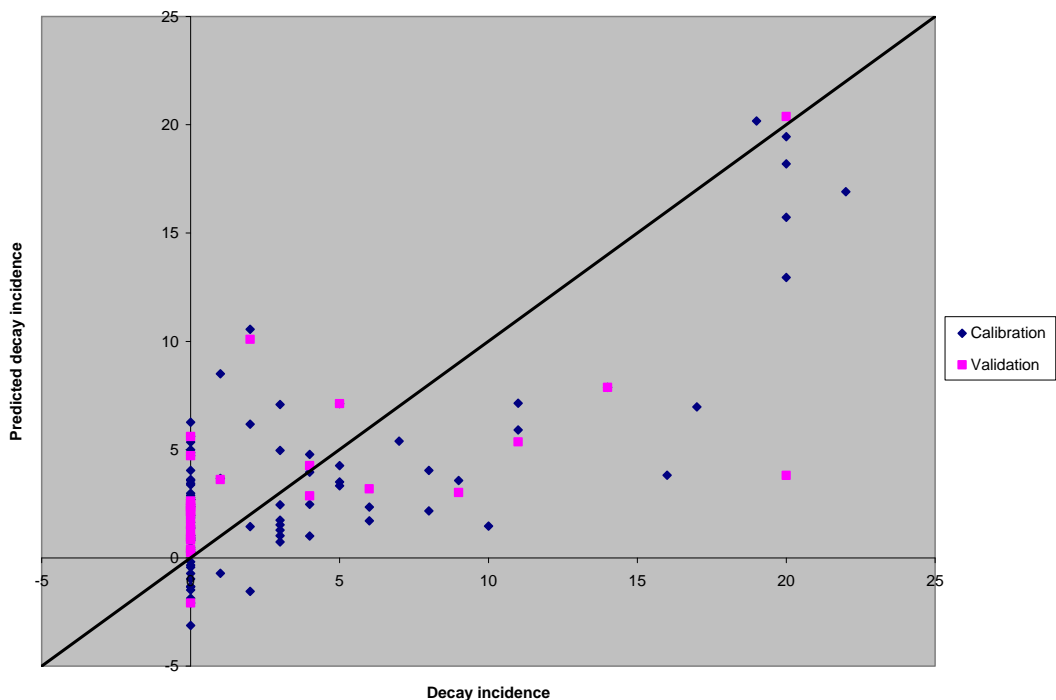


Figure 20. Predicted decay incidence vs. decay incidence (Model 28).

Nine PLS-DA models based on average decay ratings, decay incidence and decay-type incidence were developed (Table 10). Those using second-derivative spectra were best able to accurately classify samples.

Figures 21 and 23 show some separation of clear, low decay and high decay samples based on decay class and incidence of decay, respectively. The loadings (Figures 22 and 24) highlight the importance of the visible region. The scores plot for the decay type model (Figure 25) shows that red heart is separated from other samples. The loadings plot for the decay type model again shows the importance of the visible range (Figure 26). The validation data are limited for the models based on moving spectra because only 39 samples were used in the validation data set. Nevertheless, they indicate poor classification accuracy.

Table 10. Prediction statistics for PLS models from spectra obtained from moving lumber.

Model #	Rating	Scaling	Trans.	Region	PCs	Q²	Overall classification accuracy (n = 28) %	Classification accuracy of classes containing decay
32	Decay	Centre	None	300-1700	3	0.12	71	3/11
33	Decay	Centre	None	400-700	3	0.13	64	1/11
34	Decay	UV	2 nd deriv.	300-1700	2	0.15	79	5/11
35	Incidence	Centre	None	300-1700	3	0.12	71	4/12
36	Incidence	Centre	None	400-700	1	0.05	64	2/12
37	Incidence	UV	2 nd deriv.	300-1700	2	0.13	79	6/12
38	Decay Type	Centre	None	300-1700	3	0.12	79	4/9
39	Decay Type	Centre	None	400-700	3	0.16	79	3/9
40	Decay Type	UV	2 nd deriv.	300-1700	2	0.12	86	5/9

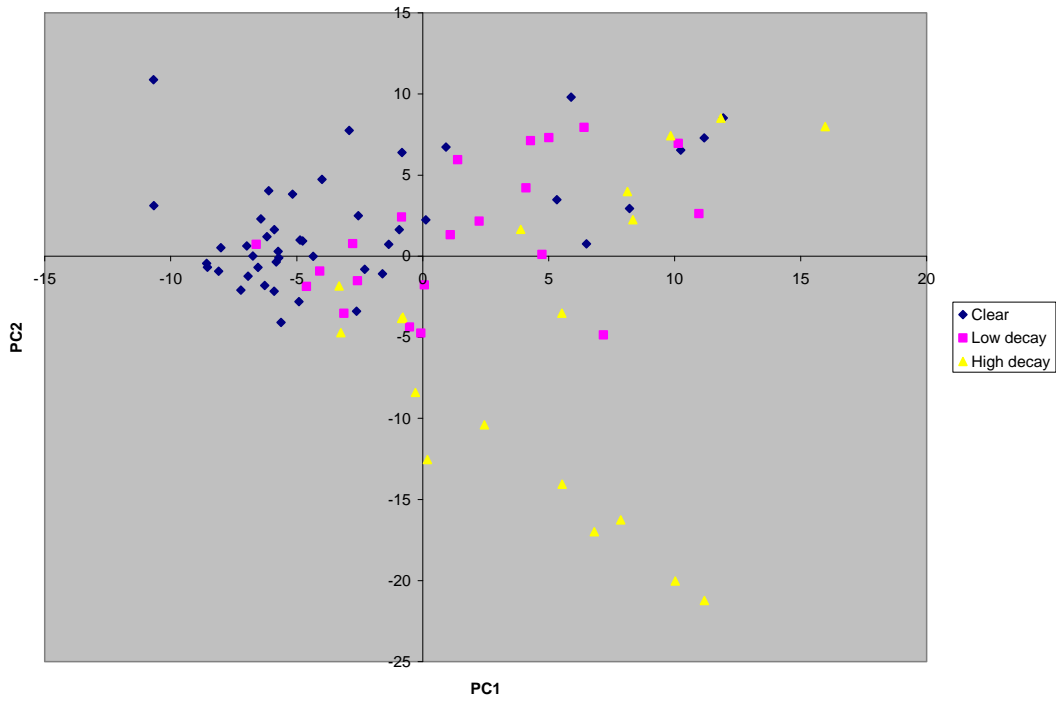


Figure 21. Scores plot from PLS-DA of decay class using second-derivative spectra obtained from moving lumber (Model 34).

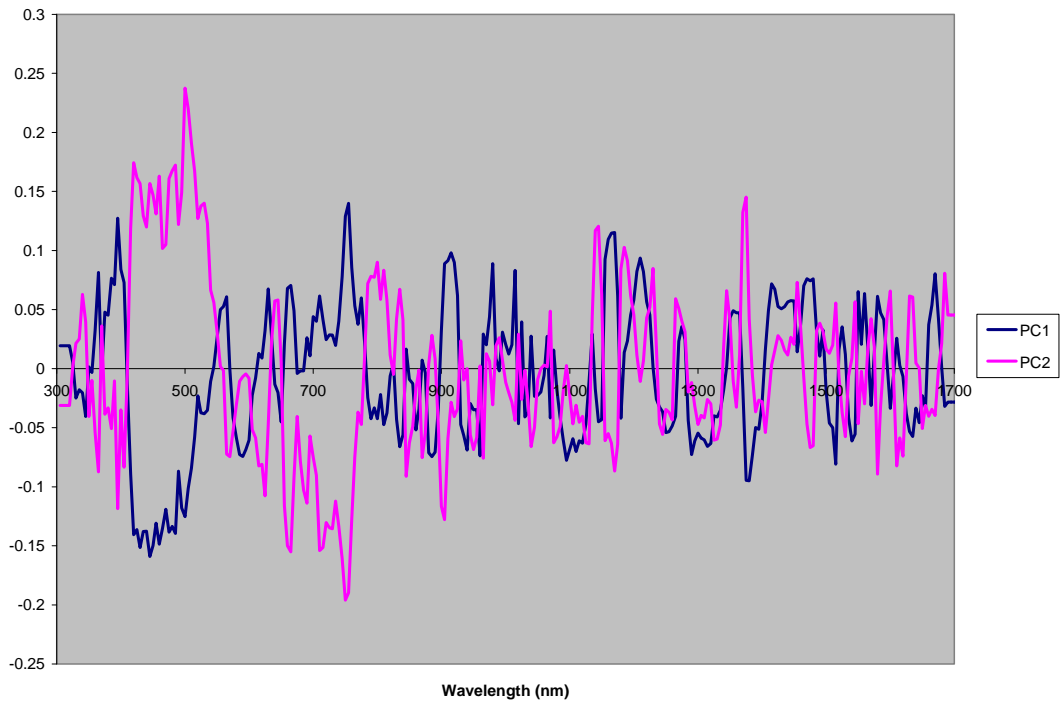


Figure 22. Loadings plot from PLS-DA of decay class using second-derivative spectra obtained from moving lumber (Model 34).

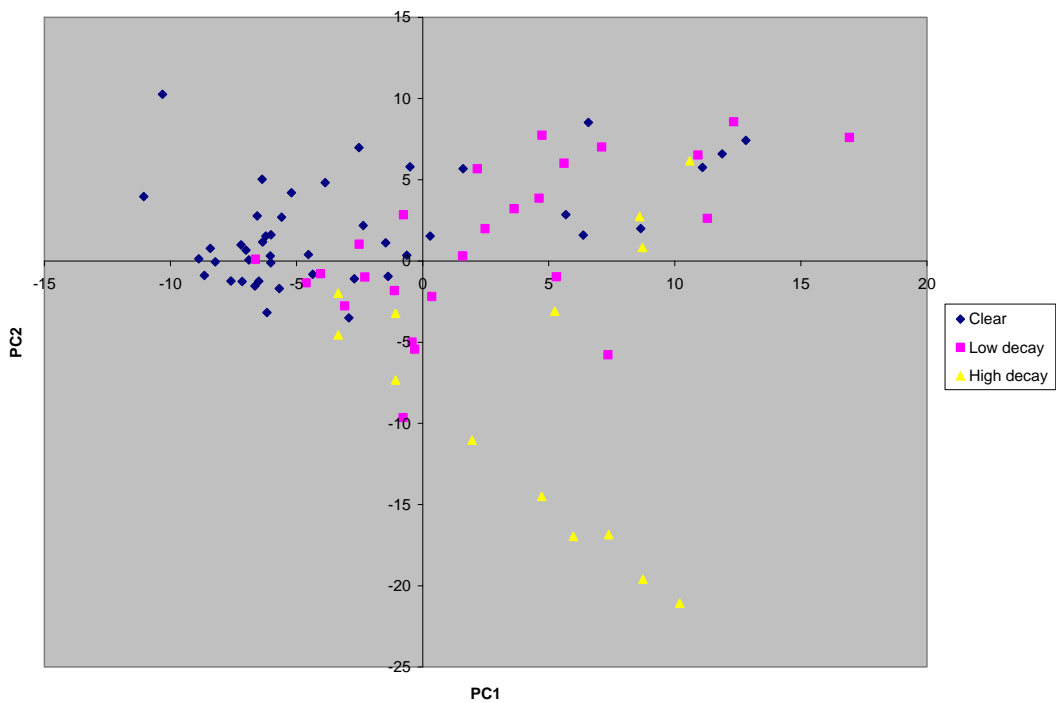


Figure 23. Scores plot from PLS-DA of incidence class using second-derivative spectra obtained from moving lumber (Model 37).

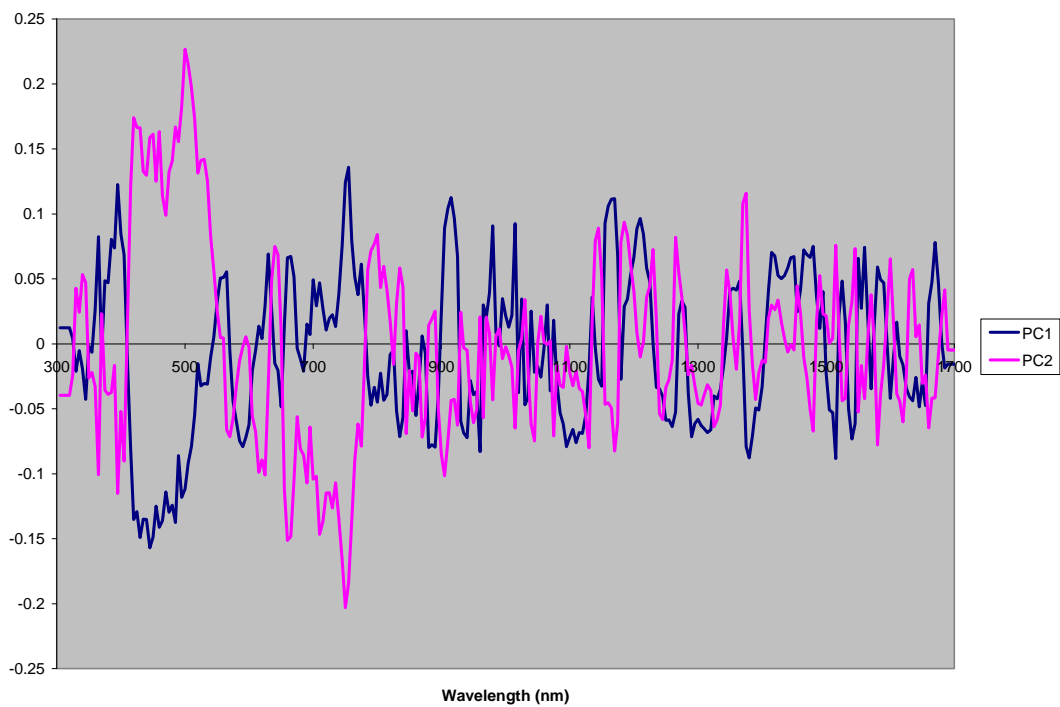


Figure 24. Loadings plot from PLS-DA of incidence class using second-derivative spectra obtained from moving lumber (Model 37).

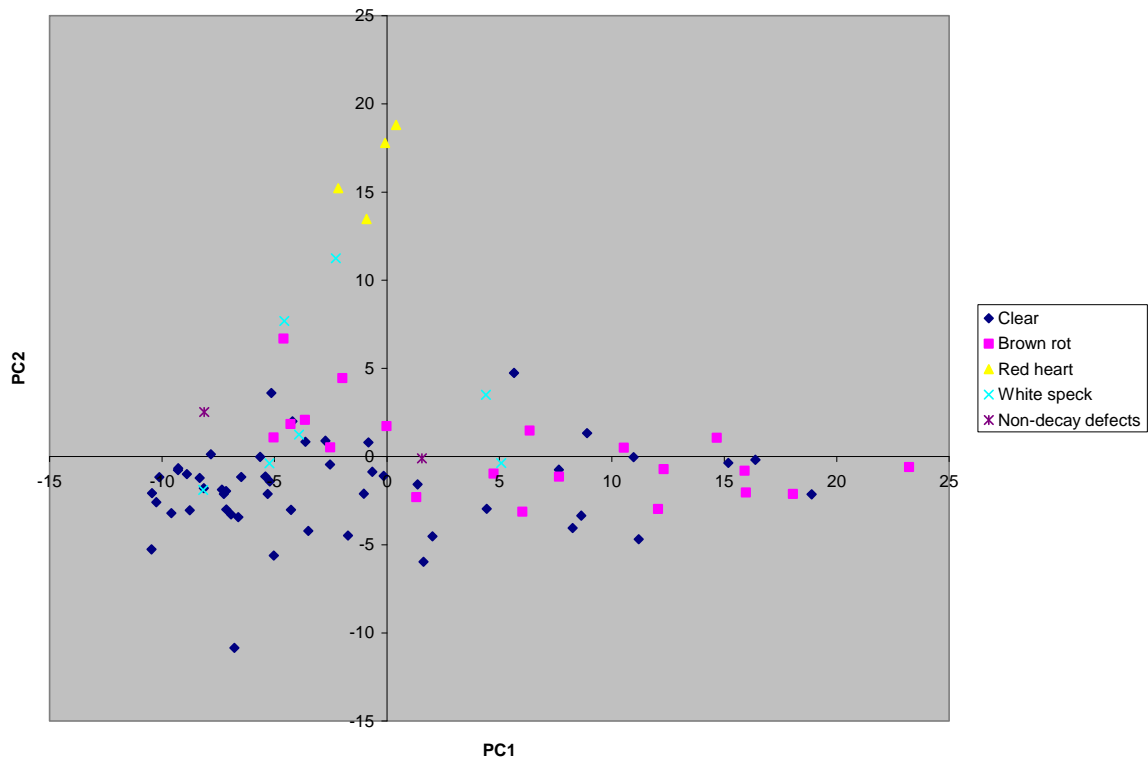


Figure 25. Scores plot from PLS-DA of decay class using second-derivative spectra obtained from moving lumber (Model 39).

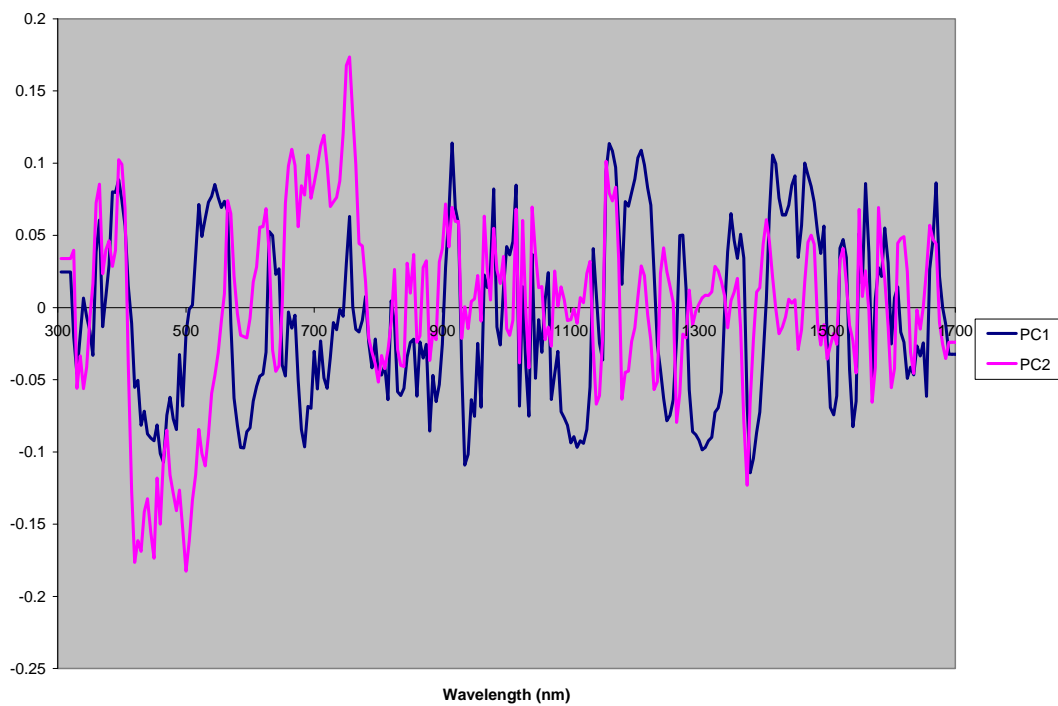


Figure 26. Loadings plot from PLS-DA of decay class using second-derivative spectra obtained from moving lumber (Model 39).

Averaged spectra from the top and bottom of each board were used to construct PLS-DA models to predict lumber grade. These models were limited by the absence of spectral data from the sides of the lumber. However, these models were able to classify boards with a reasonable degree of accuracy, despite having low Q^2 (Table 11). The scores plot for Model 42 (Figure 27) shows good separation based on lumber grade. The second derivative loadings (Figure 28) indicate that the model was based on all spectral regions and not biased towards the visible region. It is somewhat surprising that the models had some predictive ability for lumber grades, as the grading process involves many factors other than decay. However, in this set of boards, it was likely the presence of decay that resulted in the lower grades.

Table 11. Prediction statistics for lumber-grade models from spectra obtained from moving lumber

Model #	Scaling	Trans.	Region	PCs	Q^2	Overall classification accuracy (n = 14) %	Classification accuracy of utility boards (n = 9) %	Classification accuracy of #2 boards (n = 5) %
41	UV	None	300-1700	2	0.25	71	88	40
42	UV	2 nd deriv.	300-1700	2	0.29	79	78	80
43	UV	None	400-700	2	0.26	71	88	40
44	UV	2 nd deriv.	400-700	2	0.17	79	67	100

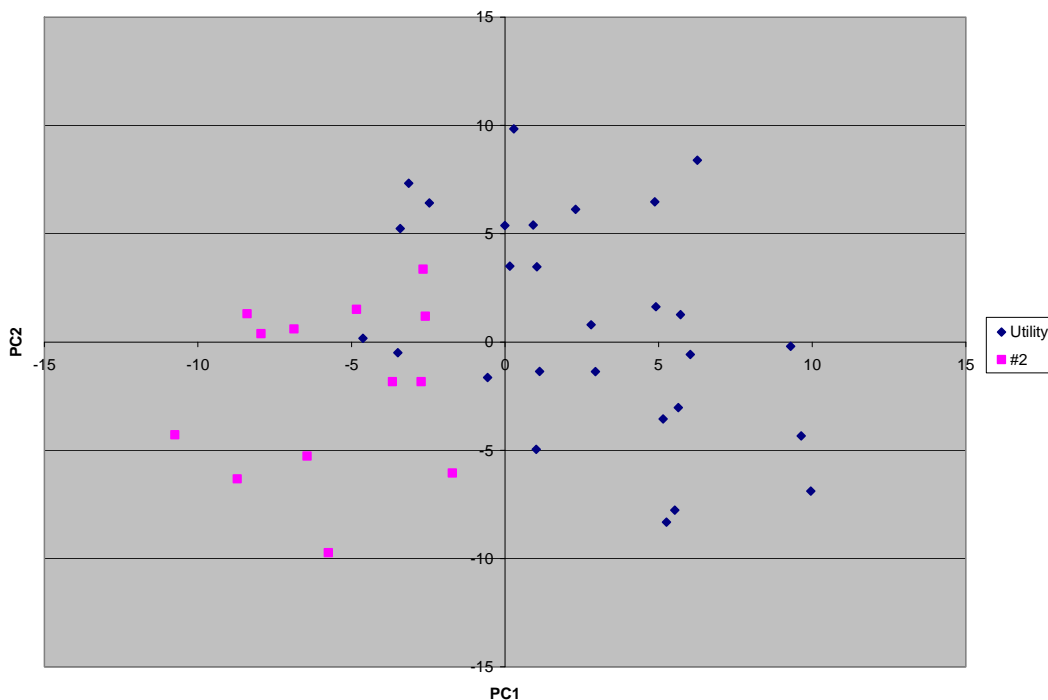


Figure 27. Scores plot from PLS-DA of grading data using second-derivative spectra obtained from moving lumber (Model 38).

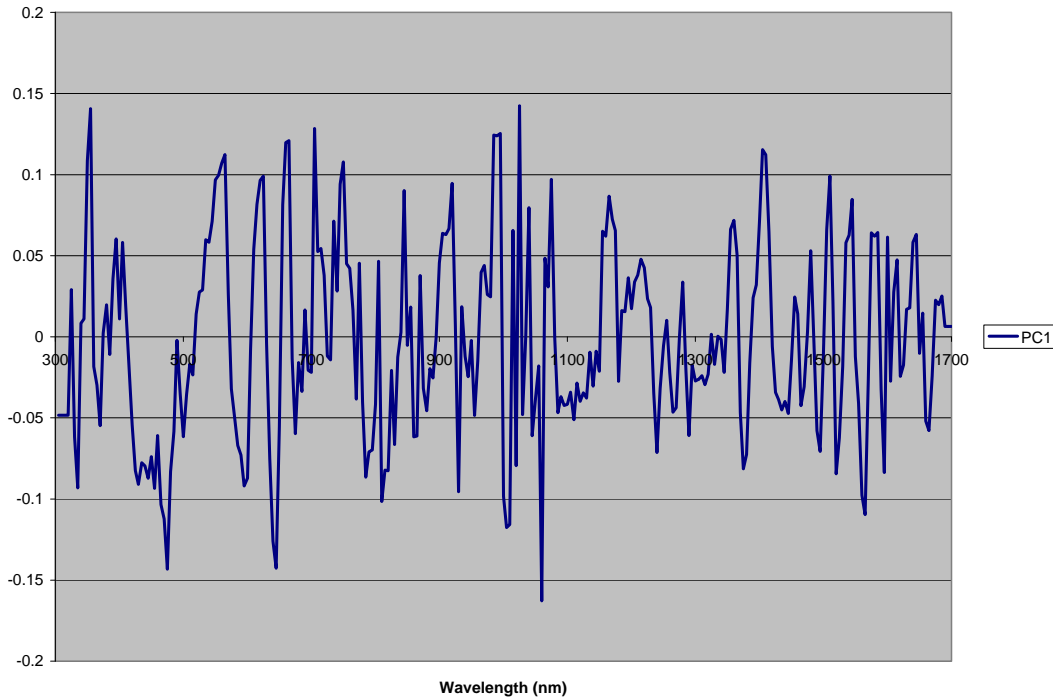


Figure 28. Loadings plot from PLS-DA of grading data using second-derivative spectra obtained from moving lumber (Model 38).

3.2.2 Higher speeds

Table 12 shows the number of spectra collected from each 2.4 m board at various conveyer speeds. There is a small range in the number of spectra collected from each board because spectra were collected continuously, and collection did not necessarily commence precisely at the beginning of each board.

Table 12. Spectra obtained from moving lumber.

Conveyer Speed (m/min)	Conveyer Speed (feet/min)	Number of Spectra Obtained	Approximate distance per spectrum (cm)
61	200	28-29	8-9
122	400	14-15	16-18
183	600	9-10	24-27
244	800	7-8	30-35

Spectral quality remained high on boards moving at all speeds. However, at higher speeds there are fewer scans per board and each scan is taken over a larger area. This reduces the spatial resolution of the spectra and the impact of a small decayed or defective region by averaging the signal from that region with adjacent sound regions.

One of the challenges of decay prediction from moving lumber, as opposed to a moving stream of chips, is the need for spectral information over small areas. The average decay content in a stream of wood chips is a process variable that could be used to alter chip furnish, or refiner or digester conditions. In contrast, the average decay content in hundreds of boards is not particularly useful, since it does not enable the

identification of individual decayed boards. At industrial speeds, spectral acquisition would need to be faster and spot size smaller to detect small patches of decay.

The sensitivity of visible or NIR data would be sufficient to detect decay in lumber if greater spatial resolution were achieved. Hyperspectral imaging combines spatial and spectral information and has been used to classify defects in food (Gowen et al. 2007) and classify pulp fibres (Tatzer et al. 2005). This type of approach has the potential to provide spectral data with high spatial resolution, which might be able to augment existing image based techniques.

None of the visible/NIR-based models detected decay more accurately than the automated grading system reported by McDonald (2008). Moreover, most of the models developed relied heavily on the visible region and not on the near-infrared region. This suggests that the addition of spectral information from the NIR region would do little to improve existing technology based on information from the visible region.

4 Conclusions

Visible/NIR spectroscopy was able to differentiate sound and decayed wood, when the spectral-collection area captured mostly uniformly sound or decayed wood. However, classification based on simple colorimetric data was almost as good as classification based on visible/NIR spectra. None of the developed models were able to detect decay more accurately than existing colour camera-based decay detection technologies. Although visible/NIR spectra are sensitive to decay, there was insufficient spatial resolution to be of use in industrial grading.

5 Acknowledgements

This project was funded by the Government of Canada through the Mountain Pine Beetle Initiative, a program administered by Natural Resources Canada, Canadian Forest Service. Publication does not necessarily signify that the contents of this report reflect the views or policies of Natural Resources Canada, Canadian Forest Service.

Thanks to Canfor Polar Division for providing the lumber used in this study. Fifty-six post-MPB kiln-dried 2.4 m 2x4s were provided by Canfor Polar Division.

The following FPInnovations staff worked obtaining lumber and rating decay, obtaining spectra and modeling decay, and writing and reviewing reports:

Paul Bicho, FPInnovations–Paprican Division;
Gordon Chow, FPInnovations–Forintek Division;
Andy Godden, FPInnovations–Forintek Division;
Dave Minchin, FPInnovations–Forintek Division;
Paul Morris, FPInnovations–Forintek Division;
Rod Stirling, FPInnovations–Forintek Division;
Lars Wallbacks, FPInnovations–Paprican Division;
Jieying Wang, FPInnovations–Forintek Division; and
Faraz Zaidi, FPInnovations–Paprican Division.

6 Contact

Rod Stirling
FPInnovations
2665 East Mall, Vancouver, BC V6T 1W5
Phone: 604-222-5712
Email: rod.stirling@fpinnovations.ca

7 Literature Cited

- (AWPA) American Wood Protection Association. 2008. E7-07. Standard method of evaluating wood preservatives by field tests with stakes. Pages 348-356 in AWPA Book of Standards. American Wood Protection Association, Birmingham, AL.
- Eriksson, L.; Johansson, E.; Kettaneh-Wold, N.; Trygg, J.; Wikström, C.; Wold, S. 2006. Page 383 in Multi- and megavariate data analysis. Part 1 Basic Principles and Applications. Umetrics, Umeå, Sweden.
- Fackler, K.; Schwanninger, M.; Grading, C.; Srebotnik, E.; Hinterstoisser, B.; Messner, K. 2007. Fungal decay of spruce and beech wood assessed by near-infrared spectroscopy in combination with uni- and multivariate data analysis. *Holzforschung* 61:680-687.
- Gowen, A.A.; O'Donnell, C.P.; Cullen, P.J.; Downey, G.; Frias, J.M. 2007. Hyperspectral imaging – An emerging process analytical tool for food quality and safety control. *Trends in Food Science and Technology* 18:590-598.
- Hoffmeyer, P.; Pedersen, J.G. 1995. Evaluation of density and strength of Norway spruce by near infrared reflectance spectroscopy. *Holz als Roh und Werkstoff* 53:165-170.
- Hsieh, E.; Uy, N.; Wallbäcks, L. 2006. Development of a portable spectroscopic sensor to measure wood and fibre properties in standing mountain pine beetle-attacked trees and decked logs. Mountain Pine Beetle Initiative Working Paper 2006-16. Natural Resources Canada, Canadian Forest Service, Victoria, BC. 33 p.
- Kelley, S.S.; Jellison, J.; Goodell, B. 2002. Use of NIR and pyrolysis-MBMS coupled with multivariate analysis for detecting chemical changes associated with brown-rot degradation of spruce wood. *FEMS Microbiology Letters* 209(1):107-111.
- Kim, J.-J.; Allen, E.A.; Humble, L.M.; Breuil, C. 2005. Ophiostomatoid and basidiomycetous fungi associated with green, red and grey lodgepole pines after mountain pine beetle (*Dendroctonus ponderosae*) infestation. *Canadian Journal of Forest Research* 35(2):274-284.
- Lewis, K.; Thompson, D.; Hartley, I.; Pasca, S. 2006. Wood decay and degradation in standing lodgepole pine (*Pinus contorta* var. *latifolia* Engelm.) killed by mountain pine beetle (*Dendroctonus ponderosa* Hopkins: Coleoptera). Mountain Pine Beetle Initiative Working Paper 2006-11. Natural Resources Canada, Canadian Forest Service, Victoria, BC. 18 p.
- McDonald, J. 2008. Assessment of automated grading systems for softwood lumber. FPInnovations–Forintek Division, Quebec City. 32 p.
- (NLGA) National Lumber Grades Authority. 2003. Standard grade rules for Canadian lumber. National Lumber Grades Authority, New Westminster, BC. 273 p.
- Savitzky, A.; Golay, M.J.E. 1964. Smoothing and differentiation of data by simplified least square procedures. *Analytical Chemistry* 36(8):1627-1639.
- Stirling, R.; Trung, T.; Breuil, C.; Bicho, P. 2007. Predicting wood decay and density using NIR spectroscopy. *Wood and Fiber Science* 39(3):414-423.
- Tatzer, P.; Wolf, M.; Panner, T. 2005. Industrial application of inline material sorting using hyperspectral imaging in the NIR range. *Real-Time Imaging* 11:99-107.